Investigation of eco-friendly double perovskites Cs_2KBiX_6 (X = Cl, Br, I) for optoelectronic and thermoelectric applications

Student ID: MS211301
Session: 2021-2022

Thesis submitted to the Department of Physics at
Jashore University of Science and Technology
in partial fulfillment of the requirements
for the degree of Masters of Science
in Physics

October 2024

Abstract

Inorganic lead free double perovskites have a wide range of applications in low cost photovoltaic and optoelectronic devices. In this study, the structural, optoelectronic, and thermoelectric properties of lead free halide double perovskites Cs_2KBiX_6 (X = Cl, Br, I) are investigated using the full potential linearized augmented plane wave (FP-LAPW) method within the density functional theory (DFT) framework, as implemented in the WIEN2k code. The structural stabilities of these materials are ensured by the negative formation energy, Goldschmidt's tolerance factor and octahedral factor. The compounds have a perfect cubic symmetry of space group $Fm\bar{3}m$ (225). The electronic configuration reveals the semiconducting nature of the compounds, with bandgaps of 4.00, 3.42, and 2.57 eV for Cs_2KBiCl_6, Cs_2KBiBr_6, and Cs_2KBiI_6 respectively. The dielectric functions, absorption coefficient, conductivity, reflectivity, and refractive index are calculated to assess the optical properties. These materials exhibit prominent absorption peaks and high optical conductivity in the ultraviolet region, indicating their suitability for optoelectronic devices such as ultraviolet sensors, detectors, and light emitting diodes (LEDs). Additionally, the BoltzTraP package is employed to determine the thermoelectric characteristics of Cs_2KBiX_6 (X = Cl, Br, I), revealing high electrical conductivity, positive Seebeck coefficient and high figure of merit. These findings suggest that the materials have promising potential for use in thermoelectric devices, including thermoelectric generators and coolers.

Acknowledgements

Firstly, I praise and thank almighty Allah, the Lord of the worlds, the Most Merciful, the Guider of hearts, the Provider of sustenance, the Owner of life and death. I want to express my gratitude to my supervisor Dr. Mohammad Abdur Rashid, for his constant support and guidance to complete my thesis properly. His knowledge and enthusiasm aided me in improving my problem solving capabilities. My sincere thanks goes to all faculty members of Department of Physics for their encouragements and insightful comments which led me to prepare for my future career. I wish to extend my profound gratitude and appreciation to the Quantum Materials Simulation Lab (QMSL) for its resources throughout the course of my thesis.

I am also thankful to all the members of the research lab for their assistance and willingness to share knowledge which has been invaluable for the quality of my work. My deepest appreciation belongs to my parents for their sacrifice and support over the years. Their love and encouragement always give me mental support to continue my study smoothly.

Contents

Investigation of eco-friendly double perovskites Cs_2KBiX_6 (X = Cl, Br, I) for optoelectronic and thermoelectric applications

List of Figures

List of Tables

Investigation of eco-friendly double perovskites Cs_2KBiX_6 (X = Cl, Br, I) for optoelectronic and thermoelectric applications

Chapter 1

Introduction

People are increasingly gravitating toward new technologies as civilization advances. Most technological progress relies on a steady and continuous supply of energy. Traditional energy sources such as fossil fuels which are limited in nature, can not keep up with the increasing energy demands driven by rapid economic growth [1–3]. Moreover, conventional energy sources are non-renewable and release various harmful gases and pollutants, posing risks to the environment and contributing to global warming [4]. In this scenario, eco-friendly renewable energy sources with a steady supply of energy are needed to tackle these problems [5]. In recent years, double perovskite materials have garnered significant attention from both theoretical and experimental perspective due to their unique properties such as tunable band gaps, high absorption coefficients, low effective masses, excellent carrier mobility and charge diffusion, and high figure of merits [6, 7]. Double perovskite materials have recently sparked significant interest due to their potential applications in a variety of disciplines, including solar cells, thermoelectric generators, light emitting diodes (LEDs), ultraviolet detectors, sensors, lasers, energy converters, and numerous other fields [8–12].

The word double perovskite is derived from the word perovskite. The term double perovskite describes a specific crystal structure that is presented by the general

formula $A_2BB'X_6$, where A stands for an alkali earth metal, B and B′ are two different transition metal and X denotes an anion [13]. Double perovskite materials with lead exhibit excellent properties due to their well-matched direct band gap, high absorption coefficient, effective masses of electrons and holes, and long carrier diffusion lengths [14–16]. Lead based perovskite are widely used in solar cells and photovoltaic devices due to their ease of fabrication and high power conversion efficiency exceeding 20% [17]. However, despite these advancements, lead-based materials are not sustainable in the long run due to their toxic impact on the environment [18]. Therefore, numerous experimental and theoretical investigations have been undertaken to adress this issue by substituting the lead with another suitable element, ensuring both efficiency and stability remain uncompromised. Alternative eco-friendly cations like bivalent Sn^{2+} and Ge^{2+} are being considered due to their similar ion radius and electronic configuration compare to bivalent Pb^{2+} [19–21]. Unfortunately, Sn^{2+} and Ge^{2+} tend to oxidize to Sn^{4+} and Ge^{4+} respectively, leading to reduced stability [22, 23]. Due to stability concerns of Sn and Ge based perovskites [24, 25] and the scarcity of suitable suitable alternative bivalent lead, trivalent cations are viable for forming double perovskites [26]. On the other hand, Slavney et al. [27] successfully synthesized $Cs_2AgBiBr_6$, a lead free bismuth based double perovskite that exhibits great promise for applications in various fields which is related to solar energy conversion, such as photovoltaic [28], photocatalytic [29], and photo-detector [30, 31]. Their findings indicate that this material possesses an indirect band gap of approximately 1.95 eV. Importantly, compared to lead based perovskites, $Cs_2AgBiBr_6$ exhibits enhanced long-term stability. The double perovskites $Cs_2AgBiCl_6$ and $Cs_2AgBiBr_6$ have been studied by McClure et al. [32] and their corresponding indirect bandgaps are reported to be 2.19 eV and 2.77 eV, respectively. This findings suggest that, both compounds remain stable in the presence of air and also explore that bismuth based double perovskite semiconductors could serve as a more environmentally sustainable option compared to lead based halide double perovskite semiconductor materials.

M. Waqas Iqbal et al. [33] conducted a study on the lead free double perovskites $K_2AgBiCl_6$ and $K_2AgBiBr_6$, which display indirect bandgaps of 2.3 eV and 1.5 eV,

respectively. Their findings suggest that, these materials are potential candidates for renewable energy fields, specially for visible light solar cells. The double perovskites K_2AgBiI_6, Rb_2AgBiI_6, and Cs_2AgBiI_6 have been investigated by Q. Mahmood et al. [34]. The reported bandgaps for these materials are 1.35 eV, 1.30 eV, and 1.26 eV, respectively which fall in the ideal range that is extremely important for solar cells. Their study also indicates that these three materials have excellent figure of merit at room temperature and most of the light energy is absorbed in visible region. So, these double perovskites materials are promising candidates for thermoelectric generators and solar cell applications. Phase diagrams and stability of lead free halide double perovskites $Cs_2BB'X_6$, where B = Sb and Bi, B′ = Cu, Ag and Au, and X = Cl, Br, and I are studied by M.R. Filip et al. [35]. Recently Shah et al. [36] has been investigated the optoelectronic and thermoelectric properties of double perovskites $Cs_2NaBiCl_6$, $Rb_2NaBiCl_6$, and $K_2NaBiCl_6$. Their studies suggest that, these materials have significant potential for optoelectronic applications such as ultraviolet sensors and detectors due to the prominant absorption peaks in ultraviolet region, low reflection and high optical conductivity and also promising for thermoelectric applications because of their high figure of merit.

Motivated by the attractive characteristics of bismuth-based double perovskites, we have used a first-principle approach and density functional theory (DFT) as implemented in WIEN2k [37, 38] code to study the structural, electrical, optical, and thermoelectric properties of Cs_2KBiX_6 (X = Cl, Br, and I). DFT [39,40] is a computational approach employed in quantum mechanics for characterizing the electronic structure and characteristics of solid materials. WIEN2k stands out as a versatile and advanced software package designed for electronic structure calculations in the field of materials science. It uses the full-potential linearized augmented plane wave (FP-LAPW) method [41]. Additionally, we use the BoltzTraP method to investigate the thermoelectric properties of Cs_2KBiX_6 (X = Cl, Br, and I) compounds. BoltzTraP is a program for calculating the semi-classic transport coefficients. It is based on a smoothed Fourier interpolation of the bands.

The arrangement of this thesis is such that in chapter 2, we discuss the basic quan-

tum mechanics as the base of density functional theory. Starting from Schrödinger equation we dispute the criteria for the ground state wave function. We shortly discuss the Born-Oppenheimar approximation and the Hartree-Fock approach with its limitations and the theoritical density functional theory in this chapter. In chapter 3, we weigh up the structural, electronic, optical and thermoelectric properties of Cs_2KBiX_6 (X = Cl, Br, and I). In last chapter, we summarize our findings on the characteristics and potential applications of the materials.

Chapter 2

Basic Quantum Mechanics

2.1 Schrödinger equation

The development of density functional theory (DFT) depends on the principles of fundamental quantum mechanics, notably the Schrödinger equation. Schrödinger equation refers to a fundamental equation of quantum physics. The Schrödinger equation is a linear partial differential equation that governs the wave function of a quantum-mechanical system [42]. It is a key result in quantum mechanics, and its discovery was a significant landmark in the development of the subject. The equation is named after Erwin Schrödinger, who postulated the equation in 1925, and published it in 1926, forming the basis for the work that resulted in his Nobel Prize in physics in 1933 [43, 44]. The time-independent Schrödinger equation

$$\hat{H}\Psi(\vec{r}) = E\Psi(\vec{r}) \tag{2.1}$$

Where, $\hat{H}$ is the hamiltonian operator and Ψ is the wave function. It is often impracticable to use a complete relativistic formulation of the formula; therefore Schrödinger himself postulated a non-relativistic approximation which is nowadays often used, especially in quantum chemistry.

Using the Hamiltonian for a single particle

$$\hat{H} = \hat{T} + \hat{V} = -\frac{\hbar^2}{2m}\vec{\nabla}^2 + V(\vec{r}) \tag{2.2}$$

leads to the (non-relativistic) time-independent single-particle Schrödinger equation

$$\hat{E}\Psi(\vec{r}) = \Big[-\frac{\hbar^2}{2m}\vec{\nabla}^2 + V(\vec{r})\Big]\Psi(\vec{r}). \tag{2.3}$$

For N particles in three dimensions, the Hamiltonian is

$$\hat{H} = \sum_{i=1}^{N} \frac{\hat{p}_i^2}{2m_i} + V(\vec{r}_1, \vec{r}_2, ...\vec{r}_N) = -\frac{\hbar^2}{2}\sum_{i=1}^{N}\frac{1}{m_i} + V(\vec{r}_1, \vec{r}_2, ...\vec{r}_N) \tag{2.4}$$

The corresponding Schrödinger equation reads

$$\hat{E}\Psi(\vec{r}_1, \vec{r}_2, ...\vec{r}_N) = \Big[-\frac{\hbar^2}{2}\sum_{i=1}^{N}\frac{1}{m_i}\nabla_i^2 + V(\vec{r}_1, \vec{r}_2, ...\vec{r}_N)\Big]\Psi(\vec{r}_1, \vec{r}_2, ...\vec{r}_N) \tag{2.5}$$

Special cases are the solutions of the time-independent Schrödinger equation, where the Hamiltonian itself has no time-dependency (which implies a time-independent potential V $(\vec{r}_1, \vec{r}_2, ..., \vec{r}_N)$ and the solutions therefore describe standing waves which are called stationary states or orbitals). The time-independent Schrödinger equation is not only easier to treat, but the knowledge of its solutions also provides crucial insight to handle the corresponding time-dependent equation.

Furthermore, the left hand side of the equation reduces to the energy eigenvalue of the Hamiltonian multiplied by the wave function, leading to the general eigenvalue equation

$$E\Psi(\vec{r}_1, \vec{r}_2, ...\vec{r}_N) = \hat{H}\Psi(\vec{r}_1, \vec{r}_2, ...\vec{r}_N) \tag{2.6}$$

Again, using the many-body Hamiltonian, the Schrödinger equation becomes

$$E\Psi(\vec{r}_1, \vec{r}_2, ..., \vec{r}_N) = \Big[-\frac{\hbar^2}{2}\sum_{i=1}^{N}\frac{1}{m_i}\nabla_i^2 + V(\vec{r}_1, \vec{r}_2, ..., \vec{r}_N)\Big]\Psi(\vec{r}_1, \vec{r}_2, ..., \vec{r}_N) \tag{2.7}$$

2.1.1 The wave function

Wave function Ψ is a quantity associated with a moving particle. It is a complex quantity. The wave function Ψ has no direct physical meaning. The wave function $\Psi(\vec{r})$ describes the position of a particle with respect to time. It can be considered as probability amplitude. $|\Psi|^2$ is proportional to the probability of finding a particle at a particular time. It is the probability density.

$$|\Psi|^2 = |\Psi^* \Psi|^2 \tag{2.8}$$

The wave function Ψ must be finite everywhere. If Ψ is finite for a particular point, it means an infinite large probability of finding the particles at that point. This would violates the uncertainty principle. It must be single valued. If Ψ has more than one value at any point, it means more than one value of probability of finding the particle at that point which is obviously ridiculous. The wave function must be continuous and have a continuous first derivative everywhere and its must be normalizable.

For the sake of simplicity the discussion is restricted to the time-independent wave function. A question always arising with physical quantities is about possible interpretations as well as observations. The Born probability interpretation of the wave function, which is a major principle of the Copenhagen interpretation of quantum mechanics, provides a physical interpretation for the square of the wave function as a probability density [45, 46]

$$P = |\psi(\vec{r}_1, \vec{r}_2, ..., \vec{r}_N|^2 d\vec{r}_1 d\vec{r}_2 .... d\vec{r}_N \tag{2.9}$$

Equation (2.10) describes the probability that particles 1,2,...,N are located simultaneously in the corresponding volume element $d\vec{r}_1\ d\vec{r}_2 ... d\vec{r}_N$ [47]. What happens if the positions of two particles are exchanged, must be considered as well. Following merely logical reasoning, the overall probability density cannot depend on such an

exchange, i.e.

$$|\Psi(\vec{r}_1, \vec{r}_2, ..., \vec{r}_i, \vec{r}_j, ..., \vec{r}_N)|^2 = |\Psi(\vec{r}_1, \vec{r}_2, ..., \vec{r}_j, \vec{r}_i, ..., \vec{r}_N)|^2 \tag{2.10}$$

There are only two possibilities for the behavior of the wave function during a particle exchange. The first one is a symmetrical wave function, which does not change due to such an exchange. This corresponds to bosons (particles with integer or zero spin). The other possibility is an anti-symmetrical wave function, where an exchange of two particles causes a sign change, which corresponds to fermions (particles which half-integer spin) [48, 49].

In this text only electrons are from interest, which are fermions. The anti symmetric fermion wave function leads to the Pauli principle, which states that no two electrons can occupy the same state, whereas state means the orbital and spin parts of the wave function [50]. The antisymmetry principle can be seen as the quantum-mechanical formalization of Pauli's theoretical ideas in the description of spectra (e.g. alkaline doublets) [51].

Another consequence of the probability interpretation is the normalization of the wave function. If equation (2.10) describes the probability of finding a particle in a volume element, setting the full range of coordinates as volume element must result in a probability of one, i.e. all particles must be found somewhere in space. This corresponds to the normalization condition for the wave function.

$$\int d\vec{r}_1 \int d\vec{r}_2 ... \int d\vec{r}_N |\psi(\vec{r}_1, \vec{r}_2, ..., \vec{r}_N)|^2 = 1 \tag{2.11}$$

Equation (2.12) also gives insight on the requirements a wave function must fulfill in order to be physical acceptable. Wave functions must be continuous over the full spatial range and square-integratable [52]. The eigenfunctions Ψ_k with corresponding energy eigenvalues are $\mathrm{E_k}$. The set Ψ_k is complete and Ψ_k may always be taken to be orthonormal and normalized

$$\int \Psi_k^* \Psi_l \; dx^N = \langle \Psi_k | \Psi_l \rangle = \delta_{kl} \tag{2.12}$$

We denote the ground state wave function and energy by Ψ_0 and E_0. Here $\int dx^N$ means integration over 3N spatial coordinates and summation over N spin coordinates. Expectation values of observables are given by formula of th type,

$$\left\langle \hat{A} \right\rangle = \frac{\int \Psi^* A \Psi \; dx}{\int \Psi^* \Psi \; dx} \tag{2.13}$$

where, $\hat{A}$ is the Hermitian linear operator for the observable A. If Ψ is normalized, expectation values of kinetic and potential energy are given by the formulas

$$T[\Psi] = \left\langle \hat{T} \right\rangle = \int \Psi^* \hat{T} \Psi \; dx \tag{2.14}$$

$$V[\Psi] = \left\langle \hat{V} \right\rangle = \int \Psi^* \hat{V} \Psi \; dx \tag{2.15}$$

When a system is in the state Ψ, which may or may not satisfy equation 2.14, the average of many measurements of the energy is given by the formula

$$E[\Psi] = \frac{\left\langle \Psi | \hat{H} | \Psi \right\rangle}{\langle \Psi \rangle} \tag{2.16}$$

where,

$$\left\langle \Psi | \hat{H} | \Psi \right\rangle = \int \Psi^* \hat{H} \Psi \; dx \tag{2.17}$$

Since furthermore, each particular measurement of the energy gives one of the eigenvalues of $\hat{H}$, we immediately have

$$E[\Psi] \geq E_0 \tag{2.18}$$

The energy computed from a guessed Ψ is an upper bound to the true ground state energy E_0. Full minimization of the functional $\mathrm{E}[\Psi]$ with respect to all allowed N-electron wae functions will give the true ground state Ψ_0 and energy $\mathrm{E}[Psi_0] = \mathrm{E}_0$,

that is,

$$E_0 = \min_{\Psi} \; E[\Psi] \tag{2.19}$$

Formal proof of minimum energy principle goes on follows. Expanding Ψ in terms of normalized eigenstates of $\hat{H}$

$$\Psi = \sum_k C_k \Psi_k \tag{2.20}$$

Then the energy becomes

$$E[\Psi] = \frac{\sum_k |C_k|^2 E_k}{\sum_k |C_k|^2} \tag{2.21}$$

where $\mathrm{E_k}$ is the energy $\mathrm{k^{th}}$ eigenstate of $\hat{H}$. Noting that the orthogonality of the Φ_k has been used. Because $\mathrm{E_0 \leq E_1 \leq ... \leq E_N}$. $\mathrm{E(\Phi)}$ is always greater than or equal to $\mathrm{E_0}$ and it reaches its minimum if and only if $\Psi = \mathrm{C_0 \Psi_0}$. Every eigenstate Ψ is an extremum of the function $\mathrm{E[\Psi]}$. In otheer words one may replace the Schrödinger equation with the variational principle

$$\delta E[\Psi] = 0 \tag{2.22}$$

when equation 2.23 is satisfied, so is equation 2.14 and vice-versa.

2.2 Born-Oppenheimer (BO) approximation

The Schrödinger equation of a many-body system is

$$H_{tot}\Psi(\{\mathbf{R}_I\}, \{\mathbf{r}_i\}) = E\Psi(\{\mathbf{R}_I\}, \{\mathbf{r}_i\}). \tag{2.23}$$

Where, H_{tot} is the total Hamiltonian, E is the total energy and $\Psi(\{\mathbf{R}_I\}, \{\mathbf{r}_i\})$ is the total wave function of the system. The total Hamiltonian of a many-body system consisting of nuclei and electrons can be written as

$$\hat{H}_{tot} = -\sum_I \frac{\hbar^2}{2M_I}\vec{\nabla}^2_{\mathbf{R}_I} - \sum_i \frac{\hbar^2}{2m_e}\vec{\nabla}^2_{\mathbf{r}_i} + \frac{1}{2}\sum_{I,J} \frac{Z_I Z_J e^2}{|\mathbf{R}_I - \mathbf{R}_J|} + \frac{1}{2}\sum_{i,j} \frac{e^2}{|\mathbf{r}_i - \mathbf{r}_j|} - \sum_{I,i} \frac{Z_I e^2}{|\mathbf{R}_I - \mathbf{r}_i|}, \tag{2.24}$$

where, the indexes I, J run on nuclei, i and j on electrons, $\mathbf{R}_I$ and M_I are position and mass of the nuclei, $\mathbf{r}_i$ and m_e are position and mass of the electrons, $|\mathbf{R}_I - \mathbf{R}_J|$, $|\mathbf{R}_I - \mathbf{r}_i|$ and $|\mathbf{r}_i - \mathbf{r}_j|$ are represent the distance between the nucleus-nucleus, nucleus-electron, and electron-electron.

As nuclei are significantly heavier than electrons (the mass of a proton is about 1836 times the mass of an electron), the electrons travel considerably more quickly than the nuclei [53]. In that case, Born-Oppenheimer (BO) approximation was proposed by Born and Oppenheimer in 1927. The Born-Oppenheimer approximation is an assumption that it is possible to distinguish equation (2.10) between the nuclear and electronic motions of molecules. After applying Born-Oppenheimer approximation, the Schrödinger equation of many body system is reduced as,

$$\hat{H}_e = -\sum_i \frac{\hbar^2}{2m_e}\vec{\nabla}^2_{\mathbf{r}_i} + \frac{1}{2}\sum_{i,j}\frac{e^2}{|\mathbf{r}_i - \mathbf{r}_j|} - \sum_{I,i}\frac{Z_I e^2}{|\mathbf{R}_I - \mathbf{r}_i|}. \tag{2.25}$$

And then the Schrödinger equation for a many body system reduces to,

$$\hat{H}\Psi = -\sum_i \frac{\hbar^2}{2m_e}\vec{\nabla}^2_{\mathbf{r}_i} + \frac{1}{2}\sum_{i,j}\frac{e^2}{|\mathbf{r}_i - \mathbf{r}_j|} - \sum_{I,i}\frac{Z_I e^2}{|\mathbf{R}_I - \mathbf{r}_i|} = E\Psi \tag{2.26}$$

The BO approximation's importance lies in it's ability to distinguish between the motion of electrons and nuclei. The starting point of DFT is the electron motion in a static external potential $V_{ext}(\mathbf{r})$ created by the nucleus.

2.3 The Hartree-Fock approach

In order to find a suitable strategy to approximate the analytically not accessible solutions of many-body problems, a very useful tool is variational calculus, similar to the least-action principle of classical mechanics. By the use of variational calculus, the ground state wave function ψ_0, which corresponds to the lowest energy of the system E_0, can be approached. A useful literature source for the principles of variational calculus has been provided by T. Flieÿbach [54].

Hence, for now only the electronic Schrödinger equation is of interest, therefore

in the following sections we set $\hat{H} \equiv \hat{H}_{el}$, $E \equiv E_{el}$, and so on. Observables in quantum mechanics are calculated as the expectation values of operators [45, 55]. The energy as observable corresponds to the Hamilton operator, therefore the energy corresponding to a general Hamiltonian can be calculated as [56]

$$E = \langle \hat{H} \rangle = \int d\vec{r}_1 \int d\vec{r}_2 ... \int d\vec{r}_N \psi * (\vec{r}_1, \vec{r}_2, ..., \vec{r}_N) \hat{H} \psi(\vec{r}_1, \vec{r}_2, ..., \vec{r}_N) \tag{2.27}$$

The Hatree-Fock techique is based on the principle that the energy obtained by any (normalized) trial wave function other than the actual ground state wave function is always an upper bound, i.e. higher than the actual ground state energy. If the trial function happens to be the desired ground state wave function, the energies are equal

$$E_{trial} \geq E_0 \tag{2.28}$$

with

$$E_{trial} = \int d\vec{r}_1 \int d\vec{r}_2 ... \int d\vec{r}_N \psi^*_{trial}(\vec{r}_1, \vec{r}_2, ..., \vec{r}_N) \hat{H} \psi_{trial}(\vec{r}_1, \vec{r}_2, ..., \vec{r}_N) \tag{2.29}$$

and

$$E_0 = \int d\vec{r}_1 \int d\vec{r}_2 ... \int d\vec{r}_N \psi^*_0(\vec{r}_1, \vec{r}_2, ..., \vec{r}_N) \hat{H} \psi_0(\vec{r}_1, \vec{r}_2, ..., \vec{r}_N) \tag{2.30}$$

The expressions above are usually inconvenient to handle. For the sake of a compact notation, in the following the bra-ket notation of Dirac is introduced. For a detailed description of this notation, the reader is referred to the original publication [57]

In that notation, equation (2.32) to (2.34) are expressed as

$$\langle \psi_{trial} | \hat{H} | \psi_{trial} \rangle = E_{trial} \geq E_0 = \langle \psi_0 | \hat{H} | \psi_0 \rangle \tag{2.31}$$

Proof [45]: The eigenfunctions ψ_i of the Hamiltonian $\hat{H}$ (each corresponding to an energy eigenvalue E_i form a complete basis set, therefore any normalized trial wave

function ψ_{trial} can be expressed as linear combination of those eigenfunctions.

$$\psi_{trial} = \sum_i \lambda_i \psi_i \tag{2.32}$$

The assumption is made that the eigenfunctions are orthogonal and normalized. Hence it is requested that the trial wave function is normalized, it follows that

$$\langle \psi_{trial} | \psi_{trial} \rangle = 1 = \langle \sum_i \lambda_i \psi_i | \sum_j \lambda_j \psi_j \rangle = \sum_i \sum_j \lambda_i^* \lambda_j \langle \psi_i | \psi_j \rangle = \sum_j |\lambda_j|^2 \tag{2.33}$$

On the other hand, following (2.35) to (2.37)

$$E_{trial} = \langle \psi_{trial} | \hat{H} | \psi_{trial} \rangle = \langle \sum_i \lambda_i \psi_i | \hat{H} | \sum_j \lambda_j \psi_j \rangle = \sum_j E_j |\lambda_j|^2 \tag{2.34}$$

Together with the fact that the ground state energy E_0 is per definition the lowest possible energy, and therefore has the smallest eigenvalue ($E_0 \leq E_i$), it is found that

$$E_{trial} = \sum_j E_j |\lambda_j|^2 \geq E_0 \sum_j |\lambda_j|^2 \tag{2.35}$$

what resembles equation (2.35).

The mathematical framework used above, i.e. rules which assign numerical values to functions, so called functionals, is also one of the main concepts in density functional theory. A function gets a numerical input and generates a numerical output whereas a functional gets a function as input and generates a numerical output [58].

Equations(2.31) to (2.39) also include that a search for the minimal energy value while applied on all allowed N-electron wave-functions will always provide the ground-state wave function (or wave functions, in case of a degenerate ground state where more than one wave function provides the minimum energy). Expressed in terms of functional calculus,where $\psi \rightarrow N$ addresses all allowed N-electron wave functions,

this means [47]

$$E_0 = \min_{\psi \to N} E[\psi] = \min_{\psi \to N} \langle \psi | \hat{H} | \psi \rangle = \min_{\psi \to N} \langle \psi | \hat{T} + \hat{V} + \hat{U} | \psi \rangle \tag{2.36}$$

Due to the vast number of alternative wave functions on the one hand and processing power and time constraints on the other, this search is essentially unfeasible for N-electron systems. Restriction of the search to a smaller subset of potential wave functions, as in the Hartree-Fock approximation, is conceivable.

A slater determinant is a formula in quantum mechanics that desceibes the wave function of a multi-fermionic system. It satisfies anti-symmetric criteria, and thus the Pauli's principle, by changing sign when two electrons are exchanged (or other fermions). Only a small fraction of all potential fermionic wave functions can be expressed as a single slater determinant, but because of their simplicity, they are an important and useful subset.

In the Hartree- Fock approach, the search is restricted to approximations of the N-electron wave function by an antisymmetric product of N (normalized) one electron wave functons, the so called spin- orbitals $\chi_i(\vec{x}_i)$ [50]. A wave function of this type is called Slater-determinant, and reads [47, 50]

$$\Psi_0 \approx \phi_{SD} = (N!)^{-\frac{1}{2}} \begin{vmatrix} \chi_1(\vec{x}_1) & \chi_2(\vec{x}_1) & \cdots & \chi_N(\vec{x}_1) \\ \chi_1(\vec{x}_2) & \chi_2(\vec{x}_2) & \cdots & \chi_N(\vec{x}_2) \\ \vdots & \vdots & \ddots & \vdots \\ \chi_1(\vec{x}_N) & \chi_2(\vec{x}_N) & \cdots & \chi_N(\vec{x}_N) \end{vmatrix} \tag{2.37}$$

It is important to notice that the spin-orbitals $\chi_i(\vec{x}_i)$ are not only depending on spatial coordinates but also on a spin coordinate which is introduced by a spin function, $\vec{x}_i = \vec{r}_i, s$. The text by Szabo [50] and Holthausen [59] omits a through description of the spin orbitals and their characteristics. Going back to the variational principle and equation 2.38, the ground state energy that can be roughly predicted by a single

determinant becomes

$$E_0 = \min_{\phi_{SD}\to N} E[\phi_{SD}] = \min_{\phi_{SD}\to N} \langle\phi_{SD}|\hat{H}|\phi_{SD}\rangle = \min_{\phi_{SD}\to N} \langle\phi_{SD}|\hat{T}+\hat{V}+\hat{U}|\phi_{SD}\rangle \quad (2.38)$$

A general expression for the Hartree-Fock Energy is obtained by usage of the Slater determinant as a trial function

$$E_0 = \langle\phi_{SD}|\hat{H}|\phi_{SD}\rangle = \langle\phi_{SD}|\hat{T}+\hat{V}+\hat{U}|\phi_{SD}\rangle \quad (2.39)$$

A general expression for the Hartree-Fock energy is obtained by uses of the slatter determinant as a trial function. According to the equation 2.34, the normalization integral $\langle\psi_{HF}|\psi_{HF}\rangle$ is equal to 1 and the energy expectation value is found to be given by formula

$$E_{HF} = \langle\psi_{HF}|\hat{H}|\psi_{HF}\rangle = \sum_i^N H_i + \frac{1}{2}\sum_i^N\sum_j^N (J_{ij} - K_{ij}) \quad (2.40)$$

where

$$H_i = \int \psi_i^*(\vec{x}_i)[-\frac{1}{2}\vec{\nabla}_i^2 + U(x)]\psi_i(\vec{x}_i)d\vec{x}, \quad (2.41)$$

$$J_{ij} = \iint \psi_i(\vec{x}_1)\psi_i^*(\vec{x}_1)\frac{1}{r_{12}}|\psi_j(\vec{x}_2)\psi_j^*(\vec{x}_2)d\vec{x}_1 d\vec{x}_2, \quad (2.42)$$

$$K_{ij} = \iint \psi_i(\vec{x}_1)\psi_j^*(\vec{x}_1)\frac{1}{r_{12}}\psi_i(\vec{x}_2)\chi_j^*(\vec{x}_2)d\vec{x}_1 d\vec{x}_2 \quad (2.43)$$

These integral are all real and $J_{ij} \geqslant K_{ij} \geqslant 0$. J_{ij} are called Coulomb integrals and K_{ij} are exchange integrals. We have the important equation

$$J_{ii} = K_{ii} \quad (2.44)$$

This is the reason the double summation in the equation that include i = j terms. Minimization of equation subject to the orthonormalization conditions,

$$\int \psi_i^*(x)\psi_j(x)dx = \delta_{ij} \quad (2.45)$$

gives the Hartree-Fock differential equation

$$\hat{F}\psi_i(x) = \sum_j^N \epsilon_{ij}\psi_j(x) \tag{2.46}$$

Where,

$$\hat{F} = -\frac{1}{2}\vec{\nabla^2} + \vec{\nu} + \vec{g} \tag{2.47}$$

In which the Coulomb exchange operator g(x_1) is given by

$$\vec{g} = \hat{j} - \hat{k} \tag{2.48}$$

Here

$$J(x_1)f(x_1) = \sum_{k=1}^N \int \psi_k^*(x_2)\psi_k(x_2\frac{1}{r_{12}}f(x_1)dx_2 \tag{2.49}$$

$$K(x_1)f(x_1) = \sum_{k=1}^* (x_2)f(x_2)\frac{1}{r_{12}}\psi_k(x_1)dx_2 \tag{2.50}$$

with f(x_1) an arbitrary function. The matrix ϵ consists of lagrange multipliers. Also,

$$\epsilon_{ji}^* = \epsilon_{ij} \tag{2.51}$$

where ϵ is Hermitian. Now multiplying this equation with ψ_i^* and integrating, one obtains the formula for orbital energies

$$\epsilon_i \equiv \epsilon_{ii} = \langle\psi_i|\hat{F}|\psi_i\rangle = H_i + \sum_{j=1}^N (\vec{J_{ij}} - \vec{K_{ij}}) \tag{2.52}$$

Summing over i and comparing with equation 2.41 we get

$$E_{HF} = \sum_{i=1}^N \epsilon_i - \hat{V_{ee}} \tag{2.53}$$

Where the symbol V_{ee} stands for electron electron repulsion energy. For the total

molecular energy including nucleus nucleus repulsion one has,

$$W_{HF} = \sum_{i=j}^{N} \epsilon_i - \hat{V_{ee}} + \hat{V_{nn}} = \sum_{i=j}^{N} H_i + \hat{V_{ee}} + \hat{V_{nn}} \tag{2.54}$$

Neither E_{HF} nor W_{HF} is equal to the sum of orbital energies. Hartree-Fock method is a non-linear self-consistent field.

2.3.1 Limitations and failings of the Hartree-Fock approach

Atoms as well as molecules can have an even or odd number of electrons. If the number of electrons is even and all of them are located in double occupied spatial orbitals ϕ_i, the compound is in a singlet state.Such systems are called closed-shell systems. Compounds with an odd number of electrons as well as compounds with single occupied orbitals, i.e. species with triplet or higher ground state, are called open-shell systems respectively. These two types of systems correspond to two different approaches of the Hartree-Fock method. In the restricted HF-method (RHF),all electrons are considered to be paired in orbitals whereas in the unrestricted HF (UHF)-method this limitation is lifted totally. It is also possible to describe open-shell systems with a RHF approach where only the single occupied orbitals are excluded which is then called a restricted open-shell HF (ROHF) which is an approach closer to reality but also more complex and therefore less popular than UHF [47].

There are also closed-shell systems which require the unrestricted approach in order to get proper results. For instance, the description of the dissociation of H_2 (i.e. the behavior at large internuclear distance), where one electron must be located at one hydrogen atom, can logically not be obtained by the use of a system which places both electrons in the same spatial orbital. Therefore the choice of method is always a very important point in HF calculations [50].

Kohn states several $M = p^5$ with $3 \leq p \leq 10$ parameters for an output with adequate accuracy in the investigations of the H_2 system [60]. For a system with N = 100

electrons, the number of parameters rises to

$$M = p^{3N} = 3^{300} to 10^{300} \approx 10^{150} to 10^{300} \tag{2.55}$$

According to the equation (2.50), energy reduction would have to be done in a space with at least 10^{150} dimension, which is well above current computer capabilities. As a result, HF methods are limited to situations involving a modest number of electron ($N \approx 10$), This barrier commonly referred to as the exponential wall because of the exponential component in (2.50) [60].

Since a many electron wave function cannot be described entirely by a single Slater determinant, the energy obtained by HF calculations is always larger than the exact ground state energy. The most accurate energy obtainable by HF-methods is called the Hartree-Fock-limit [47].

2.3.2 Correlation energy

No single determinant or straightforward combination of a few determinants can ever accurately describe the wave function for a system with many interacting electrons. The calculation of the energy error, however, is here characterized as being negative. the difference between E_{HF} and E_{exact} is called correlation energy and can be denoted as [61],

$$E_{corr}^{HF} = E_{min} - E_{HF} \tag{2.56}$$

When atomic and molecular changes preserve the number and type of chemical bonds, correlation energy tends to remain constants, but it can fluctuate significantly and become decisive when bonds change. Its magnitude can range from a few hundredths of an atomic unit to hundreds of kilocalories per mole. Exchange energies are an order magnitude or more bigger, even if the self exchange term is omitted. Despite the fact that E_{corr} is usually small against E_{min} as in the example of N_2 molecule where

$$E_{corr}^{HF} = 14.9eV < 0.001 E_{min} \tag{2.57}$$

It can have a huge influence. For instance, the experimental dissociation energy of N_2 molecule is

$$E_{diss} = 9.9eV < E_{corr} \tag{2.58}$$

which corresponds to a large contribution of the correlation energy to relative energies which are of particular interest in quantum chemistry. The mean field approximation utilized in the HF-method is what contributes most to the correlation energy. The implication of this is that one electron moves in the average field of the other ones, a method that completely ignores the inherent correlation of the electron movements. To get a better understanding what that means, one may picture the repulsion of electrons at small distances which clearly cannot be covered by a mean-field approach like the Hartree-Fock method.

2.4 The electron density

A general statement concerning the computation of observablees has been presented in section 2.1.1 about the wave function ψ. This section is about a quantity that is computed in a similar manner. The electron density (for N electrons) as the basic variable of density functional theory is defined as [47, 62]

$$n(\vec{x}) = N \sum_{s_1} \int d\vec{x}_2 ... \int d\vec{x}_N \psi^*(\vec{x}_1, \vec{x}_2, ..., \vec{x}_N)\psi(\vec{x}_1, \vec{x}_2, ..., \vec{x}_N). \tag{2.59}$$

which is the basic variable of density function theory. If the spin coordinates are neglected, the electron density can even be expressed as measurable observable only dependent on spatial coordinates [60, 62]

$$n(\vec{r}) = N \int d\vec{r}_2 ... \int d\vec{r}_N \psi^*(\vec{r}_1, \vec{r}_2, ..., \vec{r}_N)\psi(\vec{r}_1, \vec{r}_2, ..., \vec{r}_N) \tag{2.60}$$

The total number of electrons can be obtained by integration the electron density over the spatial variables [47]

$$N = \int d\vec{r} n(\vec{r}). \tag{2.61}$$

2.5 Thomas-Fermi Model

The assumptions stated by Thomas are that, electrons are distributed uniformly in a six dimentional phase space for the motion of an electron at the rate of two for each h^3 of volume and that there is an effective potential field that is itself determined by the nuclear charge and this distribution of electrons. The Thomas Fermi formula for electron density can be derived from these assumptions [63]. Let us consider the space devided into many small cubes, each of side l and volume $\Delta \mathrm{V} = l^3$, each containing some fixed number of electrons ΔN and we assume that the electrons in each shell behave like indipendent fermions at the temperature 0 K, with the cells independent of one another. The energy level of a particle in a three dimensional infinite well are given by the formula [63]

$$\epsilon(n_x, n_y, n_z) = \frac{h^2}{8ml^2}(n_x^2 + n_y^2 + n_z^2) = \frac{h^2}{8ml^2}R^2 \tag{2.62}$$

Where n_x, n_y, n_z = 1,2,3... and the second equality defines by the quantity R. For high quantum numbers, that is, for large R, the number of distinct energy levels with energy smaller than ϵ can be approximated by the volume of one octant of a spherical with radius R in the space (n_x, n_y, n_z). This number is,

$$\phi(\epsilon) = \frac{1}{8}(\frac{4\pi R^3}{3})[R = (\frac{8ml^2\epsilon}{h^2})^{\frac{3}{2}}] \tag{2.63}$$

$$= \frac{\pi}{6}(\frac{8ml^2\epsilon}{h^2})^{\frac{3}{2}} \tag{2.64}$$

The number of energy levels between ϵ and $\epsilon + \delta\epsilon$ is accordingly

$$g(\epsilon)\Delta\epsilon = \phi(\epsilon + \delta\epsilon) - \phi(\epsilon) \tag{2.65}$$

$$= \frac{\pi}{4}(\frac{8ml^2}{h^2})^{\frac{3}{2}\epsilon^{\frac{1}{2}}}\delta\epsilon + O((\delta\epsilon)^2) \tag{2.66}$$

where the function g(ϵ) is the density of states at energy ϵ. To compute the total energy for the cell with ΔN electrons, we need the probability for the state with

energy ϵ to be occupied which we call f(ϵ). This is the Fermi Dirac distribution.

$$f(\epsilon) = \frac{1}{1 + e^{\beta(\epsilon-\mu)}} \tag{2.67}$$

The Fermi energy ϵ_f is the zero temperature limit of the chemical potential μ. Now we find the total energy of the electrons in this cell by summing the contributions from the different energy states:

$$\Delta E = 2 \int \epsilon f(\epsilon) g(\epsilon) d\epsilon \tag{2.68}$$

$$= 2 \int \epsilon f(\epsilon) \frac{\pi}{4} (\frac{8ml^2}{h^2})^{\frac{3}{2}} \epsilon^{\frac{1}{2}} d\epsilon \tag{2.69}$$

$$= \frac{8\pi}{5} (\frac{2m}{h^2})^{\frac{3}{2}} l^3 \epsilon_f^{\frac{5}{2}} \tag{2.70}$$

where the factor 2 enters because each energy level is doubly occupied by one electron with spin α and another with spin β. The fermi energy E_f is related to the number of electrons ΔN in the cell through the formula

$$\Delta N = 2 \int f(\epsilon) g(\epsilon) d\epsilon \tag{2.71}$$

$$= \frac{8\pi}{3} (\frac{2m}{h^2})^{\frac{3}{2}} l^3 \epsilon_f^{\frac{3}{2}} \tag{2.72}$$

Eleminating ϵ_f from 2.71 and 2.73 we have

$$\Delta E = \frac{3}{5} \Delta N E_f \tag{2.73}$$

$$= \frac{3h^2}{10m} (\frac{3}{8\pi})^{\frac{2}{3}} l^3 (\frac{\Delta N}{l^3})^{\frac{5}{3}} \tag{2.74}$$

Equation 2.75 is a relation between total kinetic energy and the electron density $\rho = \frac{\Delta N}{l^3}$, for each cell in the space. Adding the contribution from all cells we find the total kinetic energy to be, now reverting to atomic units,

$$T_{TF}[\rho] = C_F \int \rho^{\frac{5}{3}}(\vec{r}) d\vec{r} \tag{2.75}$$

where,

$$C_F = \frac{3}{10}(3\pi^2)^{\frac{2}{3}} = 2.871 \tag{2.76}$$

Here, we first come across the LDA [64], one of the most significant concepts in contemporary density functional theory. By using locally applicable relations suited for a homogeneous electronic system, electronic characteristics are approximated as functions of the electron density. In terms of electron density, the energy formula for an atom is

$$T_{TF}[\rho(\vec{r})] = C_F \int \rho^{\frac{5}{3}}(\vec{r})d\vec{r} - Z\int \frac{\rho(\vec{r})}{\vec{r}}d\vec{r} + \frac{1}{2}\iint \frac{\rho(\vec{r_1})\rho(\vec{r_2})}{|\vec{r_1}-\vec{r_2}|}d\vec{r_1}d\vec{r_2} \tag{2.77}$$

This is the energy functional of Thomas-Fermi theory of atoms. The method became considered as an overly simplified model of little real significance for quantitative predictions in atomic, molecular, or solid state physics because the accuracy for atoms is not as high with this model as it is with other methods.

2.6 The Hohenberg-Kohn (HK) Theorems

DFT was proven to be an exact theory of many-body systems by Hohenberg and Kohn [65] in 1964. It applies not only to condensed-matter systems of electrons with fixed nuclei, but also more to any system of interacting particles in an external potential $V_{ext}(\vec{r})$. The theory is based upon two theorems.

2.6.1 HK theorem I

Statement: The ground state particle density $n(\mathbf{r})$ of a system of interacting particles in an external potential $V_{ext}(\mathbf{r})$ uniquely determines the external potential $V_{ext}(\mathbf{r})$, except for a constant. Thus the ground state particle density determines the full Hamiltonian, except for a constant shift of the energy. In principle, all the states including ground and excited states of the many-body wavefunctions can be calculated. This means that the ground state particle density uniquely determines all properties of the system completely.

Proof: Here we only consider the case that the ground state of the system is nondegenerate. It can be proven that the theorem is also valid for systems with degenerate ground state [66]. Suppose there are two different external potentials $V_{ext}(\mathbf{r})$ and $V'_{ext}(r)$ whice differ by more than a constant and lead to the same ground state density $n_0(\mathbf{r})$. The two external potentials would give two different Hamiltonians, Ψ and Ψ', with $\hat{H}\Psi = E_0\Psi$ and $\hat{H}'\Psi' = E'_0\Psi'$. Since Ψ' is not the ground state of $\hat{H}$, it follows that

$$\begin{aligned} E_0 &< \langle\Psi'|\hat{H}|\Psi'\rangle \\ &< \langle\Psi'|\hat{H}'|\Psi'\rangle + \langle\Psi'|\hat{H} - \hat{H}'|\Psi'\rangle \\ &< E'_0 + \int n_0(\mathbf{r})\Big[Vext(\mathbf{r}) - V'_{ext}(\mathbf{r})\Big]d\mathbf{r} \end{aligned} \tag{2.78}$$

Similarly

$$\begin{aligned} {E_0}' &< \langle\Psi|\hat{H}'|\Psi\rangle \\ &< \langle\Psi|\hat{H}|\Psi\rangle + \langle\Psi|\hat{H}' - \hat{H}|\Psi\rangle \\ &< E_0 + \int n_0(\mathbf{r})\Big[V'_{ext}(\mathbf{r}) - V_{ext}(\mathbf{r})\Big]d\mathbf{r} \end{aligned} \tag{2.79}$$

Adding Equations (2.57) and (2.58) lead to the contradiction

$$E_0 + E'_0 < E_0 + E'_0 \tag{2.80}$$

Hence, no two different external potentials $V_{ext}(\mathbf{r})$ can give rise to the same ground state density $n_0(\mathbf{r})$,i.e., the ground state density determines the external potential $V_{ext}(\mathbf{r})$, except for a constant.That is to say, there is a one-to-one mapping between the ground state density $n_0(\mathbf{r})$ and the external potential $V_{ext}(\mathbf{r})$, although the exact formula is known.

2.6.2 HK theorem II

Statement: There exists a universal functional $F[n(\mathbf{r})]$ of the density, independent of external potential $V_{ext}(\mathbf{r})$, such that the global minimum value of the energy functional $E[n(\mathbf{r})] \equiv \int n(\mathbf{r})V_{ext}(\mathbf{r})d(\mathbf{r}) + F[n(\mathbf{r})]$ is the exact ground state energy of the system and the exact ground state density $n_0(\mathbf{r})$ minimizes this functional. Thus the exact ground state energy and density are fully determined by the functional $E[n(\mathbf{r})]$.

Proof: The universal functional $F[n(\mathbf{r})]$ can be written as

$$F[n(\mathbf{r})] \equiv T[n(\mathbf{r})] + E_{int}[n(\mathbf{r})] \tag{2.81}$$

where $T[n(\mathbf{r})]$ is the kinetic energy and $E_int[n(\mathbf{r})]$ is the interaction energy of the particles. According to variational principle, for any wave function Ψ', the energy functional $E[\Psi']$:

$$E[\Psi'] = \langle \Psi' | \hat{T} + \hat{V}_{int} + \hat{V}_{ext} | \Psi' \rangle \tag{2.82}$$

has its global minimum value only when Ψ' is the ground state wave function Ψ_0, with the constraint that the total number of the particles is conserved. According to HK theorem I, Ψ' must correspond to a ground state with particle functional of $n'(\mathbf{r})$ and external potential $V'_{ext}(\mathbf{r})$, then $E[\Psi']$ is a functional of $n'(\mathbf{r})$. According to variational principle:

$$\begin{aligned} E[\Psi'] \equiv \langle \Psi' | \hat{T} + \hat{V}_{int} + \hat{V}_{ext} | \Psi' \rangle = E[n'(\mathbf{r})] = \int n'(\mathbf{r}) V'_{ext}(\mathbf{r}) d\mathbf{r} + F[n'(\mathbf{r})] \\ > E[\Psi_0] \\ = \int n_0(\mathbf{r}) d(\mathbf{r}) + F[n_0(\mathbf{r})] = E[n_0(\mathbf{r})] \end{aligned} \tag{2.83}$$

Thus the energy functional $E[n(\mathbf{r})] \equiv \int n(\mathbf{r})V_{ext}(\mathbf{r})d(\mathbf{r}) + F[n(\mathbf{r})]$ evaluated for the correct ground state density $n_0(\mathbf{r})$ is indeed lower than the value of this functional for any other density $n(\mathbf{r})$. Therefore by minimizing the total energy functional of the system with respect to variations in the density $n(\mathbf{r})$, one would find the exact ground state density and energy.

2.7 Kohn-Sham (KS) equation

An inventive indirect method of monoelectronic equation for the kinetic-energy functional $T[n(\mathbf{r})]$ was developed by Kohn and Sham in 1965 as Kohn-Sham (KS) method [67]. Kohn and Sham proposed introducing orbitals into the problem in such a way that the kinetic energy can be computed simply to good accuracy, leaving a small residual correction that is handled separately. It is convenient to begin with the exact formula for the ground-state kinetic energy,

$$T = \sum_{i}^{N} a_i \langle \psi_i | -\frac{1}{2}\nabla^2 | \psi_i \rangle \tag{2.84}$$

where, ψ_i and a_i respectively, natural spin orbitals and their occupation numbers. We are assured from the Hohenberg-Kohn theory that this T is a functional of the total electron density.

$$n(\mathbf{r}) = \sum_{i}^{N} a_i |\psi_i(\mathbf{r})|^2 \tag{2.85}$$

Kohn and Sham showed that one can built a theory using simpler formulas, namely,

$$T_s[n] = \sum_{i}^{N} \langle \psi_i | -\frac{1}{2}\nabla^2 | \psi_i \rangle \tag{2.86}$$

and

$$n(\mathbf{r}) = \sum_{i}^{N} |\psi_i(\mathbf{r})|^2 \tag{2.87}$$

This representation of kinetic energy and density holds true for the determinantal wave function that exactly describes N non-interacting electrons. In analogy with the Hohenberg-Kohn defination of the universal functional $F_{HK}[n]$, Kohn and Sham invoked a corresponding non-interacting reference system, with the Hamiltonian,

$$\hat{H}_s = \sum_{i}^{N} (\frac{1}{2}\nabla_i^2) + \sum_{i}^{N} v_s \tag{2.88}$$

in which there are no electron-electron repulsion terms and for which the ground state electron density is exactly n. For this system, there will be an exact determi-

nantal ground-state wave function,

$$\psi_s = \frac{1}{\sqrt{N!}}\, det[\psi_1\psi_2 \dots \psi_N] \tag{2.89}$$

where ψ_i are the N lowest eigenstates of the one-electron Hamiltonian $\hat{H}_s$:

$$\hat{H}_s\psi_i = [-\frac{1}{2}\nabla^2 + v_s(\mathbf{r})]\psi_i = \varepsilon_i\psi_i \tag{2.90}$$

The kinetic energy is $T_s[n]$, given by equation (2.40)

$$T_s[n] = \langle\psi_s|\sum_i^N(-\frac{1}{2}\nabla_i^2)|\psi_s\rangle = \sum_{i=1}^N\langle\psi_i| - \frac{1}{2}\nabla^2|\psi_i\rangle \tag{2.91}$$

and the density is decomposed as in equation (2.41). The forgoing definition of $T_s[n]$ leaves an undesirable restriction on the density. Its need to be non interacting v representable. That is, there must exist a non interacting ground state with the given density $n(\mathbf{r})$. This restriction on the domain of definition of $T_s[n]$ can be lifted and $T_s[n]$ of the form of equation (2.40) can be defined for any density derived from an antisymmetric wave function. The quantity $T_s[n]$, although uniquely defined for any density, is still not the exact kinetic energy functional. Kohn-Sham set up a problem of interest in such a way that $T_s[n]$ is it's kinetic energy component. To produce the desired separation out of $T_s[n]$ as the kinetic energy component, we write the equation as

$$F[n] = T_s[n] + J[n] + E_{xc}[n]. \tag{2.92}$$

Where,

$$E_{xc}[n] = T[n] - T_s[n] + V_{ee}[n] - J[n] \tag{2.93}$$

Here the defined quantity $\mathrm{E_{xc}[n]}$ is called exchange-correlation energy. It contains the difference between T and T_s, presumably fairly small and non-classical part of $V_{ee}[n]$. The Euler equation then can be written in terms of effective potential

$$\mu = v_{eff}(\mathbf{r}) + \frac{\delta T_s[n]}{\delta n(\mathbf{r})} \tag{2.94}$$

Where v_{eff} effective potential is defined by

$$v_{eff}(\mathbf{r}) = v(\mathbf{r}) + \frac{\delta J[n]}{\delta n(\mathbf{r})} + \frac{\delta E_{xc}[n]}{\delta n(\mathbf{r})} = v(\mathbf{r}) + \int \frac{n(\mathbf{r}')}{|\mathbf{r} - \mathbf{r}'|} dr' + V_{xc}(\mathbf{r}) \tag{2.95}$$

with the exchange-correlation potential which is given by,

$$V_{xc}(\mathbf{r}) = \frac{\delta E_{xc}[n]}{\delta n(\mathbf{r})} \tag{2.96}$$

For a system of non-interacting electrons moving in the external potential $\mathrm{V_s}(\mathbf{r}) = \mathrm{V_{eff}}(\mathbf{r})$. Therefore, for a given $\mathrm{V_s}(\mathbf{r})$, one obtains the $n(\mathbf{r})$ that satisfies eq.(2.60) simply by solving the N-one electron equations,

$$[-\frac{1}{2}\nabla^2 + v_{eff}(\mathbf{r})]\psi_i = \varepsilon_i \psi_i \tag{2.97}$$

where ε_i is the eigenvalue of monoelectron equation and setting

$$n(\mathbf{r}) = \sum_i^N |\psi_i(\mathbf{r})|^2 \tag{2.98}$$

In above two equations the solutions ψ_i can be different this is because equations are non linear and must be solved iteratively. The total energy can be determined from the resultant density via equation

$$E[n] = T_s[n] + J[n] + E_{xc}[n] + \int n(\mathbf{r}) V(\mathbf{r}) d(\mathbf{r}) \tag{2.99}$$

Hence,

$$\sum_i^N \varepsilon_i = \sum_i^N \langle \psi_i | \sum_i^N (-\frac{1}{2}\nabla_i^2) + V_{eff}(\mathbf{r}) | \psi_i \rangle \tag{2.100}$$

$$= T_s[n] + \int V_{eff}(\mathbf{r}) n(\mathbf{r}) d(\mathbf{r}) \tag{2.101}$$

Just as in Hatree-Fock theory, the total electronic energy is not the sum of the orbital energies.

2.7.1 Solving Kohn-Sham equation

In a condensed matter system the Kohn Sham (KS) equation gives a way to obtain the exact density and energy of the ground state. The process starts with an initial electron density n(r), usually a superposition of atomic electron density, then the effective potential V_{eff} is calculated and the KS equation is solved with single-particle eigenvalues and wavefunctions, a new electron density is then calculated from the wavefunctions.

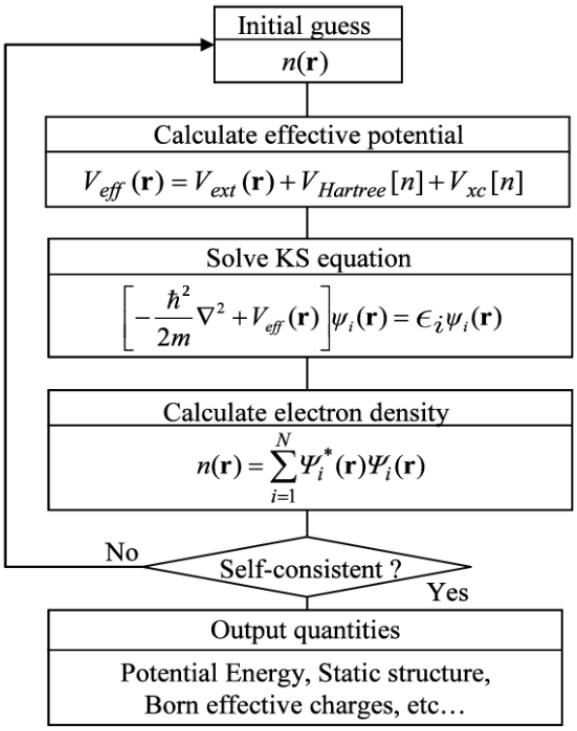

Figure 2.1: Flowchart of self-consistency loop for solving Kohn-Sham equations

This is usually done numerically through some self-consistent iteration as shown in above flowchart. Self-consistent condition can be the change of total energy or electron density from the previous iteration or total force acting on atoms is less than some chosen small quantity, or a combination of these individual conditions. If self-consistency is not achieved, the calculated electron density will be mixed with electron density from previous iterations to get a new electron density. A new iteration will start with the new electron density. This process continues until self-consistency is reached. After the self-consistency is reached, various quantities can

be calculated including total energy, forces, stress, eigenvalues, electron density of states, band structure, etc..

2.8 Local Density Appeoximation (LDA)

The Khon Sham equation while exactly incorporating the kinetic energy $T_s[\rho]$, still leave the exchange correlational functional $E_xc[\rho]$ unsetteled. In Khon Sham equation let us introduce the local density approximation proposed by Khon and Sham. The kinetic energy $T_s[\rho]$ is regorously treated in the Kohn Sham schame, we can use the uniform electron gas formula solely for the unknown part of the rest of the energy functional. Thus we introduce the local density approximation (LDA) for exchange and correlation energy.

$$E_{xc}^{LDA}[\rho] = \int \rho(\vec{r})\epsilon_{xc}(\rho)d\vec{r} \tag{2.102}$$

Where $\epsilon_{xc}[\rho]$ indicates the exchange and correlation energy per particle of a uniform electron gas of density ρ. The corresponding exchange correlation potential then becomes,

$$V_{xc}^{LDA}(\vec{r}) = \frac{\delta E_{xc}^{LDA}[\rho]}{\delta\rho(\vec{r})} \tag{2.103}$$

$$= \epsilon_{xc}(\rho(\vec{r})) + \rho(\vec{r})\frac{\delta E_{xc}[\rho]}{\delta\rho(\vec{r})} \tag{2.104}$$

and the Khon Sham orbital equations read,

$$[-\frac{1}{2}\vec{\nabla}^2 + V(\vec{r}) + \int \frac{\rho(\vec{r})}{|\vec{r}-\vec{r'}|}d\vec{r'} + V_{xc}^{LDA}(\vec{r})]\psi = \epsilon_i\psi_i \tag{2.105}$$

This self consistent solution defines the KS local density approximation, which is the literature is usually simply called Local Density Approximation (LDA) method. The function $\epsilon_{xc}(\rho)$ can be devided into exchange and correation contributions,

$$\epsilon_{xc}(\rho) = \epsilon_x(\rho) + \epsilon_c(\rho) \tag{2.106}$$

The exchange part is already known given by the Dirac exchange energy functional.

$$\epsilon_x(\rho) = -C_x\rho^{\frac{1}{3}}(\vec{r}) \tag{2.107}$$

where

$$C_x = \frac{3}{4}(\frac{3}{\pi})^{\frac{1}{3}} \tag{2.108}$$

2.9 Local Spin Density Approximation (LSDA)

The spin-density-functional theory is the necessary generalization for systems in the presence of an external magnetic field. It is also exceedingly important for systems in the absence of a magnetic field, because it allows one to build more physics into the approximate exchange-correlation functional through its spin dependence. In the presence of a magnetic field $B(\vec{r})$ that acts only on the spins of the electrons, the Hamiltonian of the system becomes,

$$H = -\frac{1}{2}\sum_i^N \nabla_i^2 + \sum_i^N V(\vec{r}) + \sum_{i<1}^N \frac{1}{\vec{r_{ij}}} + 2\beta_e \sum_i^N B(\vec{r}).\vec{S_i} \tag{2.109}$$

Where, $\beta_e = \frac{e\hbar}{2mc}$ is the Bohr magneton and $\vec{S_i}$ is the electron angular momentum vectorfor the $i^{t\hbar}$ electron. The added magnetic interaction is still a one-electron operator, just like the nuclear potential $V(\vec{r})$. We can combine terms in the following convenient way:

$$\hat{V} = \sum_i^N V(\vec{r_i}) + 2\beta_e \sum_i^N B(\vec{r}).\vec{S_i} \tag{2.110}$$

$$= \int v(\vec{r})\hat{n}(\vec{r})d\vec{r} - \int B(\vec{r})\hat{m}(\vec{r})d\vec{r} \tag{2.111}$$

where $\hat{n}(\vec{r})$ is the operator for electron density,

$$\hat{n}(\vec{r}) = \sum_i^N \delta(\vec{r} - \vec{r_i}) \tag{2.112}$$

and and $\hat{m}(\vec{r})$ is the operator for the electron magnetization density,

$$\hat{m}(\vec{r}) = -2\beta_e \sum_i^N S_i \delta(\vec{r} - \vec{r_i}) \tag{2.113}$$

Both $\hat{n}(\vec{r})$ and $\hat{m}(\vec{r})$ are local operators. The expectation value of $\hat{V}$ for the state $|\psi\rangle$ is given by,

$$\langle\psi|\hat{V}|\psi = \int v(\vec{r})n(\vec{r})d\vec{r} - \int B(\vec{r})m(\vec{r})d\vec{r} \tag{2.114}$$

where the electron density is given by,

$$n(\vec{r}) = \langle\psi|\hat{n}(\vec{r})|\psi\rangle \tag{2.115}$$

and the magnetization density by,

$$m(\vec{r}) = \langle\psi|\hat{m}(\vec{r})|\psi\rangle \tag{2.116}$$

We shall discuss only the simple case of z-direction $b(\vec{r})$. We then have,

$$\langle\psi|\hat{V}|\psi\rangle = \int v(\vec{r})n(\vec{r})d\vec{r} - \int b(\vec{r})m(\vec{r})d\vec{r} \tag{2.117}$$

where

$$\begin{aligned} m(\vec{r}) &= -2\beta_e\langle\psi| \sum_i^N S_z(i)\delta(\vec{r} - \vec{r_i})|\psi\rangle \\ &= \beta_e[n^\beta(\vec{r}) - n^\alpha(\vec{r})] \end{aligned} \tag{2.118}$$

We obtain the spin-density-functional theory by breaking the minimum search for the ground-state energy into two steps. Namely,

$$E_0 = \min_\psi \langle\psi|T + V_{ee} + \sum_i^N U(\vec{r_i}) + 2\beta_e \sum_i^N b(\vec{r_i}).S_z(i)|\psi\rangle \tag{2.119}$$

$$= \min_{n^\alpha, n^\beta}\{\min_{\psi\to n^\alpha, n^\beta}\langle\psi|T + V_{ee}\rangle + \int[v(\vec{r})n(\vec{r}) - \int b(\vec{r})m(\vec{r})]d\vec{r}\} \tag{2.120}$$

$$= \min_{n^\alpha, n^\beta}\{F[n^\alpha, n^\beta] + \int[(V(\vec{r}) - \beta_e b(\vec{r}))n^\alpha(\vec{r}) + \beta_e b(\vec{r}))n^\beta(\vec{r})]d\vec{r}\} \tag{2.121}$$

where

$$F[n^\alpha, n^\beta] = \min_{\psi \to n^\alpha, n^\beta} \langle \psi | T + V_{ee} | \psi \rangle \tag{2.122}$$

This provides constrained-search formulation of the universal functional $F[n^\alpha, n^\beta]$. The functional $F[n^\alpha, n^\beta]$ searches all ψ that yield the input $n^\alpha(\vec{r})$ and $n^\beta(\vec{r})$, then $F[n^\alpha, n^\beta]$ assumes the minimum of $\langle F + V_{ee} \rangle$. The last equality of (8.1.10) is the basis of the spin-density-functional theory: n^α and n^β are all that are needed to describe the ground state of the many-electron system in the presence of a magnetic field $b(\vec{r})$. However, $F[n^\alpha, n^\beta]$ is unknown, and approximation is necessary for the theory to be implemented.

The Kohn-Sham method can now be introduced to rigorously handle the kinetic energy contribution to $F[n^\alpha, n^\beta]$,

$$F[n^\alpha, n^\beta] = T_s[n^\alpha, n^\beta] + J[n^\alpha + n^\beta] + E_{xc}[n^\alpha, n^\beta] \tag{2.123}$$

where $T_s[n^\alpha, n^\beta]$ is the Kohn-Sham kinetic-energy functional corresponding to a system of non-interacting electrons with densities n^α and n^β and $E_{xc}[n^\alpha, n^\beta]$ is the exchange correlation energy functional. A constrained search definition of T_s can also be given,

$$T_s[n^\alpha, n^\beta] = min \sum_{i\alpha} n_{i\alpha} \int d\vec{r} \phi^*_{i\alpha}(\vec{r}) (\frac{1}{2}\nabla^2) \phi_{i\alpha} \vec{r} \tag{2.124}$$

where the minimization is over the set of $n_{i\alpha}$ and $\phi_{i\alpha}$, with constraints,

$$\sum_i n_{i\alpha} |\phi_{i\alpha}(\vec{r})|^2 = n^\alpha(\vec{r}) \tag{2.125}$$

$$\sum_i n_{i\beta} |\phi_{i\beta}(\vec{r})|^2 = n^\beta(\vec{r}) \tag{2.126}$$

We may express the energy (3.55) as a functional of the orbitals $\phi_{i\alpha}$,

$$\begin{aligned} E[n^\alpha, n^\beta] = &\sum_{i\alpha} n_{i\alpha} \int d\vec{r} \phi^*_{i\alpha}(\vec{r}) (-\frac{1}{2}\nabla^2) \phi_{i\alpha} \vec{r} + J[n^\alpha + n^\beta] + E_{xc}[n^\alpha, n^\beta] \\ &+ \int [(V(\vec{r}) + \beta_e b(\vec{r})) n^\alpha(\vec{r}) + (V(\vec{r}) - \beta_e b(\vec{r})) n^\beta(\vec{r})] d(\vec{r}) \end{aligned} \tag{2.127}$$

The variational search for the minimum of $E[n^\alpha, n^\beta]$ can then be carried out through orbitals, subject to normalization constraints,

$$\int \phi^*_{i\alpha}(\vec{r})\phi_{i\alpha}(\vec{r})d\vec{r} = 1 \tag{2.128}$$

The resulting Kohn-Sham equations are,

$$\hat{h}^\alpha_{eff}\phi_{i\alpha}(\vec{r}) = [-\frac{1}{2}\nabla^2 + V^\alpha_{eff}]\phi_{i\alpha}(\vec{r}) = \epsilon_{i\alpha}\phi_{i\alpha}(\vec{r}) \tag{2.129}$$

and

$$\hat{h}^\beta_{eff}\phi_{j\beta}(\vec{r}) = [-\frac{1}{2}\nabla^2 + V^\beta_{eff}]\phi_{j\beta}(\vec{r}) = \epsilon_{j\beta}\phi_{j\beta}(\vec{r}) \tag{2.130}$$

where the spin-dependent effective potentials are,

$$v^\alpha_{eff}(\vec{r}) = v(\vec{r}) + \int \frac{n(\vec{r})}{|\vec{r} - \vec{r'}|d\vec{r}} + \frac{\delta E_{xc}[n^\alpha, n^\beta]}{\delta n^\alpha(\vec{r})} + \beta_e b(\vec{r}) \tag{2.131}$$

$$v^\beta_{eff}(\vec{r}) = v(\vec{r}) + \int \frac{n(\vec{r})}{|\vec{r} - \vec{r'}|d\vec{r}} + \frac{\delta E_{xc}[n^\alpha, n^\beta]}{\delta n^\beta(\vec{r})} + \beta_e b(\vec{r}) \tag{2.132}$$

In equations (3.65) and (3.66), the number of electrons with α spin and β spin,

$$N^\alpha = \int n^\alpha(\vec{r})d\vec{r} \tag{2.133}$$

and

$$N^\beta = \int n^\beta(\vec{r})d\vec{r} \tag{2.134}$$

need also to be varried to achieve minimum total energy under the constraint,

$$N = N^\alpha + N^\beta \tag{2.135}$$

With the spin-polarized Kohn-Sham equations, the kinetic energy is handled exactly and only the exchange-correlation energy remains to be determined. The exchange-

correlation contribution can be separated into exchange and correlation pieces,

$$E_{xc}[n^\alpha, n^\beta] = E_x[n^\alpha, n^\beta] + E_c[n^\alpha, n^\beta] \tag{2.136}$$

where the exchange part is defined as,

$$E_x[n^\alpha, n^\beta] = -\frac{1}{2}\int\int \frac{1}{\vec{r}_{12}}\{|n_1^{\alpha,\alpha}(\vec{r_1}, \vec{r_2})|^2 + |n_1^{\beta,\beta}(\vec{r_1}, \vec{r_2})|^2\} d\vec{r_1}\vec{r_2} \tag{2.137}$$

with

$$n_1^{\alpha,\alpha}(\vec{r_1}, \vec{r_2}) = \sum_i n_{i\alpha}\phi_{i\alpha}(\vec{r_1})\phi_{i\alpha}^*(\vec{r_2}) \tag{2.138}$$

$$n_1^{\beta,\beta}(\vec{r_1}, \vec{r_2}) = \sum_i n_{i\beta}\phi_{i\beta}(\vec{r_1})\phi_{i\beta}^*(\vec{r_2}) \tag{2.139}$$

The $n_{i\alpha}$ and $\phi_{i\alpha}$ are those giving the Kohn-Sham kinetic energy, they are determined by p^α and p^β.

$$E_x[n^\alpha, n^\beta] = \frac{1}{2}E_x[n^\alpha, n^\alpha] + \frac{1}{2}E_x[n^\beta, n^\beta] \tag{2.140}$$

$$= \frac{1}{2}E_x^0[2n^\alpha] + \frac{1}{2}E_x^0[2n^\beta] \tag{2.141}$$

where

$$E_x^0[n] = E_x[\frac{1}{2}n, \frac{1}{2}n] \tag{2.142}$$

The Dirac local-density approximation (LDA) for exchange is for the spin-compensated case. Thus from above equations, we obtain the local spin-density approximation (LSDA) for the exchange energy functional,

$$E_x^{LSDA}[n^\alpha, n^\beta] = 2^{\frac{1}{3}}C_x\int[(n^\alpha)^{\frac{4}{3}} + (n^\beta)^{\frac{4}{3}}]d\vec{r} \tag{2.143}$$

2.10 Generalized Gradient Approximations (GGA)

The LSDA neglects inhonogeneities of real charge density which could be deffer-ent from the Homogeneous Electron Gas (HEG). The exchange correlation energy density has significantly different result from HEG. This gives rise to the various

Generalized-Gradient Approximations (GGA) [68] which include density gradient correlation and higher spatial dertiviatives of electron density and gives better result than LDA in many cases. Three most widely used GGA's are the from propeosed by Becke [69], Perdew et al. [70] and Perdew, Burke and Enzerhof. For spin polarized system [71] we know that

$$E_{XC}^{LSDA}[n\uparrow(r), n\downarrow(r)] = \int n(r)\epsilon_{XC}^{h}om(n\uparrow(r), n\downarrow(r))dr \tag{2.144}$$

Where XC energy density $\epsilon_{XC}^{h}om$(n(r)) is a function of the density alone and is decomposed into exchange energy density $\epsilon_{X}^{h}om$(n(r)) and correlation energy density $\epsilon_{C}^{h}om$(n(r)) . So that the XC energy functional is decomposed into exchange energy functional E_{X}^{LDA}[n(r)] and correlation energy functional E_{C}^{LDA}[n(r)] linearly. From density gradient $\nabla n(r)$,

$$E_{XC}^{GGA}[[n\uparrow(r), n\downarrow(r)] = \int n(r)\epsilon_{XC}^{h}om(n\uparrow(r), n\downarrow(r), |\nabla n\uparrow(r)|, |\nabla n\downarrow(r)|...)dr \tag{2.145}$$

$$= \int n(r)\epsilon_{X}^{h}omn(r)F_{XC}(n\uparrow(r), n\downarrow(r), |\nabla n\uparrow(r)|, |\nabla n\downarrow(r)|...)dr \tag{2.146}$$

Where, F_{XC} is a dimensionless and ϵ_{X}^{hom}n(r) is the exchange energy density of the unpolarized HEG. F_{XC} can be decomposed linearly into exchange contribution F_c as $F_{XC} = F_x + F_c$. Generally GGA works better than LDA, in pridicting binding energy of molecules and bond length, crystal lattice constants, especially the system where charge density varried rapidly. In case of ionic crystall, GGA overcorrects LDA results where the lattice constants of LDA fit well than GGA. But in case of transition metal oxides and rare-earth element, both LDA and GGA parform badly. This drawback leads to approximations beyond LDA and GGA.

2.11 Meta-GGA

In density functional theory (DFT), meta-generalized gradient approximation (meta-GGA) [72] is an extension of the traditional generalized gradient approximation (GGA) exchange-correlation functionals. Meta-GGA functionals aim to improve

the accuracy of DFT calculations by considering not only the electron density but also the gradient of the electron density and the kinetic energy density. The meta-GGA functionals typically include additional terms beyond those found in GGA functionals, which allows for a more refined description of the electronic system. These functionals can capture non-local effects and better account for long-range correlations, leading to improved predictions of various properties, such as structural parameters, energetics, and spectroscopic properties. The meta-GGA exchange-correlation functional is generally represented as

$$E_{meta-GGA} = \rho(\vec{r})\epsilon_{meta-GGA}(\vec{r}d\vec{r}) \tag{2.147}$$

where, $E_{meta-GGA}$ is the meta-GGA exchange correlation energy functional, $\rho(\vec{r})$ is the electron density at position r, and $\epsilon_{meta-GGA(\vec{r})}$ is the meta-GGA exchange correlation density functional at position r. The specific form of meta-GGA functionals can vary depending on the proposed functional. Common meta-GGA functionals include TPSS (Tao, Perdew, Staroverov, and Scuseria) [72], M06-L (Zhao and Truhlar) [73], and MS2 (Sun, Ruzsinszky, and Perdew) [74], among others. These functionals introduce additional density functionals, kinetic energy density functionals, and density gradient functionals to better capture the electronic behavior. It's important to note that meta-GGA functionals require careful parameterization and testing for different systems to ensure their accuracy and reliability. The performance of meta-GGA functionals can vary depending on the system under investigation, and some functionals may be more suitable for specific applications than others.

2.12 LDA+U method

The systems which are strongly correlated contain rare-earth metal (transition metal) having partially filled d or f shells. LSDA and GGA can not explain them properly. In this method, electrons are considered into two classes: delocalized s, p electron and localized d or f electrons. The total energy in LSDA+U [75] method is given

by,

$$E_{tot}^{LDA+U}[\rho_\sigma(r), n_\sigma] = E^{LSDA}[\rho_\sigma(r)] + E^{U}[n_\sigma] - E_{dc}[n_\sigma] \tag{2.148}$$

where, σ = spin indexes

$\rho_\sigma(r)$ = electron density for spin-σ electrons.

n_σ = density matrix of f or d electron for spin-σ electrons

$E^{LSDA}[\rho_\sigma(r)]$ = standard LSDA energy functional

$E^{U}[n_\sigma]$ = electron-electron coulomb interaction energy. The last term is double counting term which remove the average LDA energy contribution of d or f electrons from the LDA energy

$$E_{dc}[n_\sigma] = \frac{1}{2}UN(N-1) - \frac{1}{2}J[N\uparrow(N\uparrow -1) + N\downarrow(N\downarrow -1)] \tag{2.149}$$

where, $N = N\uparrow + N\downarrow$. U and J are Coulomb and exchange parameters. If exchange and non sphericity is neglected then,

$$E_{tot}^{LDA+U} = E_{LDA} + \frac{1}{2}U\sum_{i\neq j} n_i n_j - \frac{1}{2}UN(N-1) \tag{2.150}$$

The orbital energies ϵ_i are derivative of above equation with respect to orbital occupations n_i

$$\epsilon_i = \frac{\partial E}{\partial n_i} = \epsilon_{LDA} + U(\frac{1}{2} - n_i) \tag{2.151}$$

For $n_i = 1$, LDA orbital energies are shifted by -$\frac{U}{2}$ and by $\frac{U}{2}$ for unoccupied orbitals ($n_i = 0$), resulting the upper and lower Hubbard bands, which opens a gap at the fermi energy in transition metal oxides. In case of double counting term, it has two different treatment: AMF and FLL. The former is most suitable for small U system [76] and the letter for large U system [77]. The energies for double counting is given by [78],

$$E_{AMF}^{dc} = \frac{1}{2}UN^2 - \frac{U+2lJ}{2l+1}\frac{1}{2}\sum_\sigma N_\sigma^2 \tag{2.152}$$

$$E_{AMF}^{dc} = \frac{1}{2}UN(N-1) - \frac{1}{2}J\sum_\sigma N_\sigma(N_{\sigma-1} \tag{2.153}$$

where, $\frac{N}{2(2l+1)}$ = average occupation of the correlated orbitals
$\frac{N_\sigma}{2l+1}$ = average occupation of a single spin of the correlated orbital.

2.13 Hybrid functionals

Hybrid functionals are a class of density functional theory (DFT) methods that aim to improve upon the accuracy of standard DFT calculations by incorporating a portion of exact or semi-exact exchange into the exchange-correlation functional. This hybrid approach combines the computational efficiency of DFT with a more accurate treatment of electronic interactions. In standard DFT, the exchange-correlation functional is typically approximated using local density approximation (LDA) or generalized gradient approximation (GGA). However, these approximations may not fully capture the exact exchange and correlation effects, leading to limitations in the accuracy of calculated properties.

To address these limitations, hybrid functionals introduce a fraction of exact or semi-exact exchange into the exchange-correlation functional. The exchange-correlation energy (E_{xc}) of a hybrid functional is expressed as a combination of the exchange energy from a non-local exchange term (E_x) and the correlation energy (E_c) from a local or semi-local functional:

$$E_{xc} = \alpha E_x + (1 - \alpha) E_c \tag{2.154}$$

Here, α is the mixing parameter that determines the amount of exact exchange included in the functional. The range of α typically varies from 0 to 1, representing pure local or semi-local functionals ($\alpha = 0$) to pure exact exchange functionals ($\alpha = 1$). The choice of the specific hybrid functional determines the form of the exchange term, and various hybrid functionals have been developed. One of the most widely used hybrid functionals is the popular B3LYP functional, which combines the Becke's three-parameter exchange functional (B3) with the Lee, Yang, and Parr correlation functional (LYP).

Hybrid functionals can improve the description of a range of properties, including

structural parameters, energetics, reaction barriers, and electronic properties such as band gaps and ionization potentials. By incorporating a portion of exact exchange, hybrid functionals provide a better balance between the delocalization and localization of electrons, capturing both short-range and long-range interactions more accurately. While hybrid functionals offer improved accuracy, they come at a higher computational cost compared to standard DFT calculations. The inclusion of exact exchange introduces non-local terms that require additional computational resources.

Chapter 3

Optoelectronic and Thermoelectric Properties of Cs_2KBiX_6

Ab-initio simulation based on density functional theory as implemented in the WIEN2k code [37,38], was used to study the structural, electronic, optical properties and BoltzTraP [79] method was used to compute the thermoelectric characteristics of Cs_2KBiX_6 (X = Cl, Br, I) halide double perovskites. This BoltzTraP method relies on the well-known Boltzmann transport theory. The exchange correlation functional was produced using the Perdew-Burke-Ernzerhof (PBE) [80] generalized gradient approximation (GGA) for solving the Kohn-Sham equations [81]. First of all, the structures of Cs_2KBiCl_6, Cs_2KBiBr_6, and Cs_2KBiI_6 were optimized, meaning that both volume and geometry optimizations were carried out in order to determine the optimum lattice constants and atomic positions for each compound respectively. For attaining best convergence, a 15 × 15 × 15 k-mesh was selected in Brillouin zone. For the iteration procedure, the limits for energy convergence and charge convergence were set as 0.00001 Ry and 0.001 e, respectively for all the studied systems. For non-overlapping spheres, the radii of the muffin-tin for all calculations were chosen to be 2.25, 2.03, 2.35, 2.00, 2.05, and 2.07 a.u. for Cs, K, Bi, Cl, Br, and I respectively. The plane wave cut-off parameter $R_{MT} \times K_{max} = 8$ was chosen,

where, R_{MT} is the smallest radius of muffin-tin sphere and K_{max} is the largest reciprocal lattice vector. Additionally, the maximum value of Gaussian-factor (G_{max}) and angular momentum vector (l_{max}) were chosen to be 16 and 10, respectively.

3.1 Crystal structure optimization

The primitive unit cell of the double perovskites Cs_2KBiX_6 (X = Cl, Br, I), as shown in Figure 3.1, indicates that the studied compounds possess a face-centered cubic structures with space group $Fm\bar{3}m$ (225). In the unit cell structure, Cs atoms have a face-centered positons with an 8c Wyckoff site and fractional coordinates (0.25, 0.25, 0.25), the K atoms are located in the corner positions with 4a Wyckoff site and fractional coordinates (0, 0, 0), Bi atoms have a body-centered positions with a 4b Wckoff site and fractional coordinates (0.5, 0.5, 0.5), and Cl/Br/I atoms have face-centered positions with a 24e Wyckoff site and fractional coordinates (0.2633/0.2622/0.2615, 0, 0). Figures 3.2 illustrate the volume vs energy optimization graphs for Cs_2KBiCl_6, Cs_2KBiBr_6, and Cs_2KBiI_6 respectively. The ground

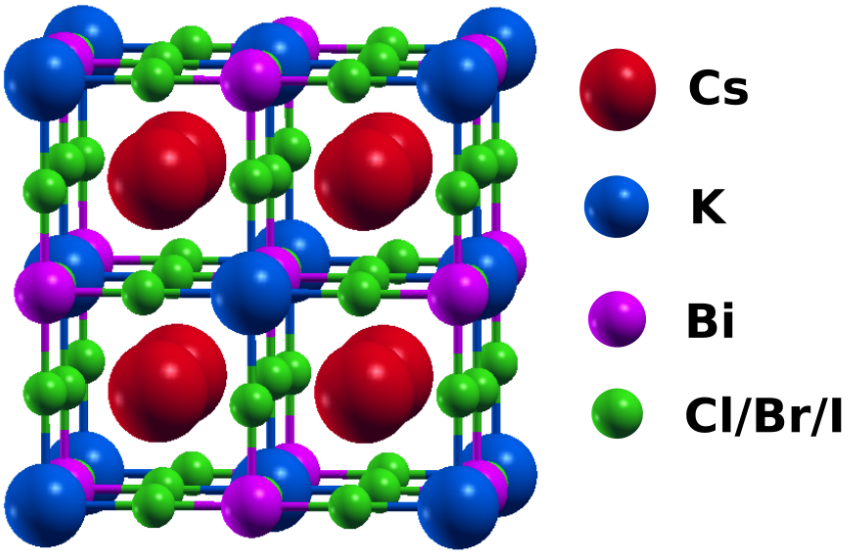

Figure 3.1: Cubic unit cell of halide double perovskites Cs_2KBiX_6 (X = Cl, Br, I).

state energy (E_0) are obtained corresponding to volume using Birch-Murnaghan's equation of states [82], which provides information about the optimized lattice constant. The optimized lattice constants (a_0) are estimated to be 11.51 Å, 12.08 Å,

and 12.94 Å for Cs_2KBiCl_6, Cs_2KBiBr_6, and Cs_2KBiI_6 respectively. The values of lattice constants increases as we change the anion from Cl to Br to I due to increase in their atomic size. The minimum optimized unit cell volume increases as we substitute Cl with Br and I due to the addition of more energy levels. The optimized structural parameters are listed in Table 3.1.

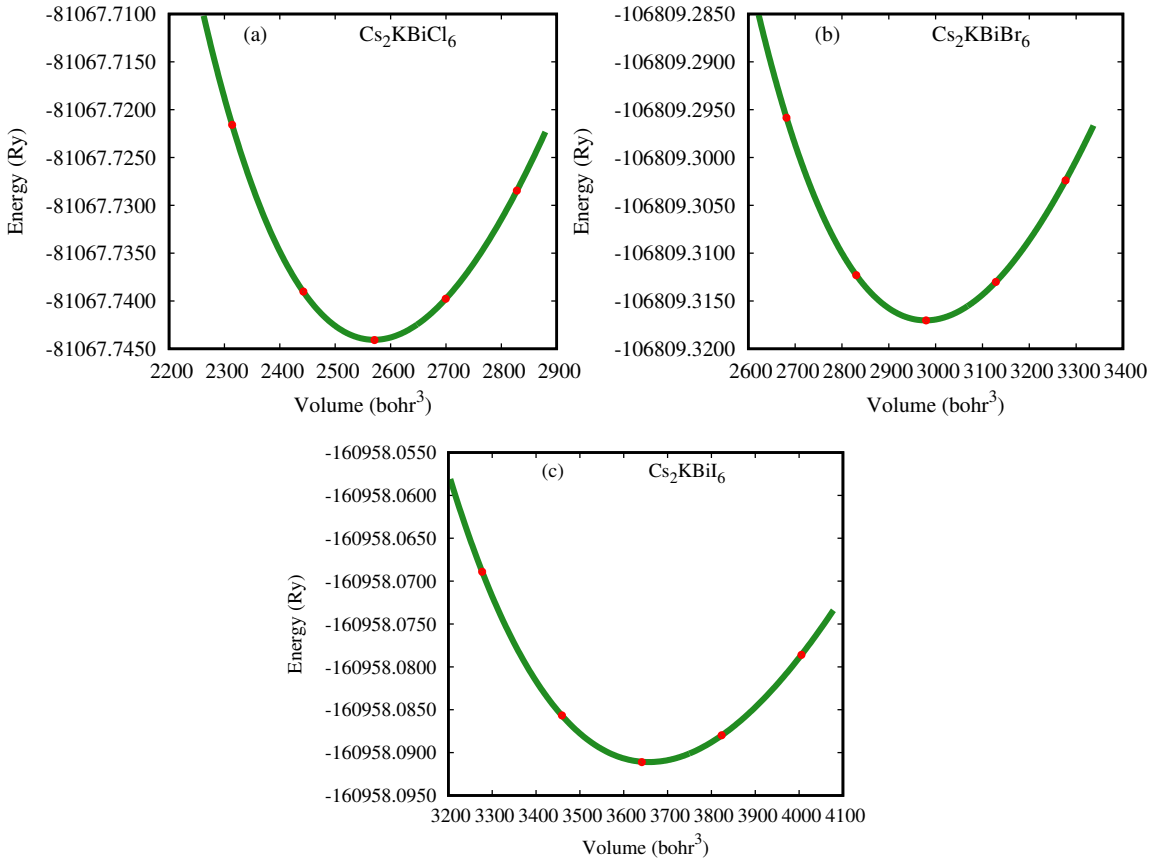

Figure 3.2: Energy versus volume curves for Cs_2KBiX_6 (X = Cl, Br, I).

The formation energy is crucial in determining the stability and reactivity of compounds. It is the energy needed to create a substance from its elements in their standard states. The following equation is utilized to compute the formation energy (ΔH) [83]

$$\Delta H = \frac{E(Cs_2KBiX_6) - 2E(Cs) - E(K) - E(Bi) - 6E(X)}{10} \tag{3.1}$$

Where, ΔH is the formation energy, $E(Cs_2KBiX_6)$ is the total energy of the sys-

tems, $E(Cs), E(K), E(Bi), E(X = Cl, Br, I)$ are the total energy of the compounds involved in perovskite decomposition reaction. The formation energy are found to be -2.08 eV, -1.69 eV and -1.27 eV for Cs_2KBiCl_6, Cs_2KBiBr_6 and Cs_2KBiI_6 respectively. The negative formation energy indicates the thermodynamic stability of the studied compounds. The stability of the compounds is further analyzed through the calculation of tolerance factor (τ) and the octahedral factor (μ) [84] are defined as,

$$\tau = \frac{r_A + r_X}{\sqrt{2}(r_B + r_X)} \tag{3.2}$$

$$\mu = \frac{r_B}{r_X} \tag{3.3}$$

In this case, r_A is the ionic radius of Cs ion, r_B is the average of the ionic radii of K and Bi, and and r_X is the ionic radius of Cl/Br/I ions. Studying by Li et al. [85,86] indicates that stable double perovskites generally exhibit tolerance factors ranging from 0.71 to 1.00 and octahedral factors ranging from 0.42 to 0.75. The calculated values of tolerance factors were 0.83, 0.82, and 0.81, and the octahedral factors were 0.65, 0.61, and 0.54 for Cs_2KBiCl_6, Cs_2KBiBr_6, and Cs_2KBiI_6 respectively. Therefore it is clear that, the studied compounds have stable structures.

3.2 Electronic properties

We investigated the electronic properties of Cs_2KBiX_6 (X = Cl, Br, I), by analyzing their band structures and density of states using the PBE-GGA functional. Among these compounds, Cs_2KBiCl_6 and Cs_2KBiBr_6 exhibit direct bandgaps of 4.00 eV and 3.42 eV respectively, because both the valence band maxima (VBM) and conduction band minima (CBM) lie at the same symmetry point L, whereas Cs_2KBiI_6 shows an indirect bandgap of 2.57 eV due to the bands lie at different symmetry points, such as conduction band minima lies at L symmetry while valence band maxima lies at Γ symmetry, as illustrated in Figure 3.3 and these bandgap values are listed in Table 3.1. Substituting the X-site anion with Cl, Br, and I sequentially decreases the bandgap, which correlates with the atomic size of these anions. Being large in

atomic size iodine contains large number of nucleons as compared to Br and Cl.

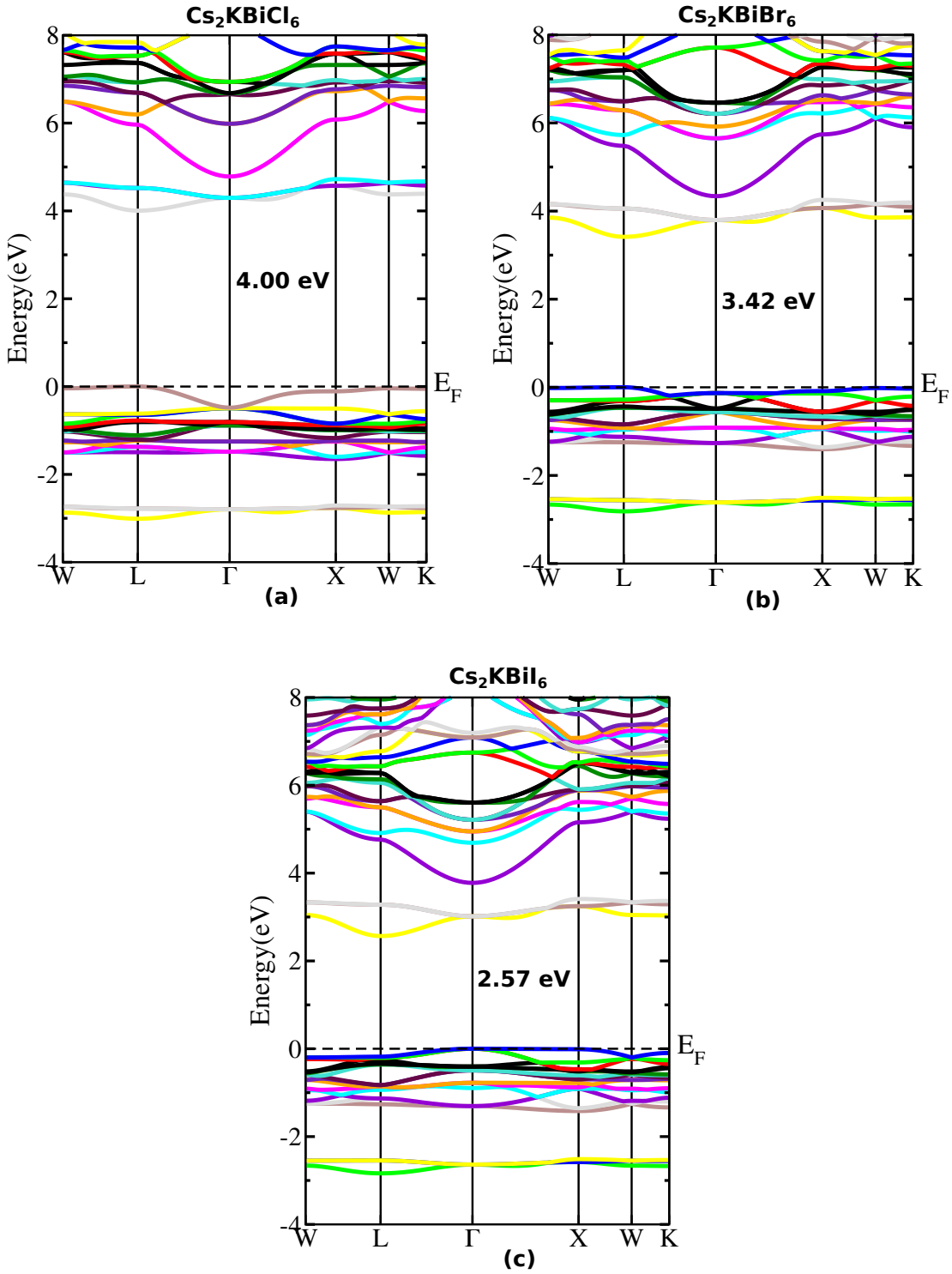

Figure 3.3: The calculated band structures of double perovskites (a) Cs_2KBiCl_6, (b) Cs_2KBiBr_6 and (c) Cs_2KBiI_6.

The replacement of large size anion at X-site decreases the electrostatic force on outer electrons. Due to the weak electrostatic force, both the bonding energy and the gap between the conduction band and valence band decrease which reduces the bandgap. In order to analyze the contribution of various electronic states of Cs_2KBiX_6 (X = Cl, Br, I), total density of states (TDOS) and partial density of states (PDOS) has been calculated which are presented in Figure 3.4 and 3.5. In these figures, the region to the left of the dotted line represents the valence band (VB), while the region to the right represents the conduction band (CB).

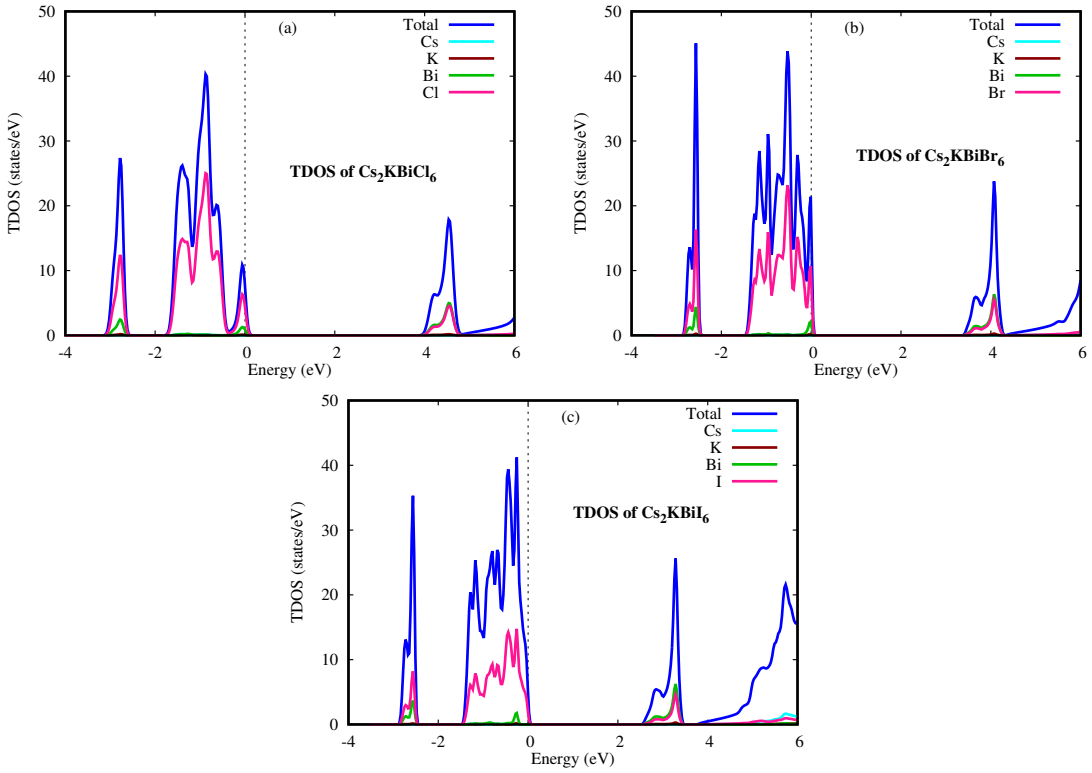

Figure 3.4: Total density of states of double perovskites Cs_2KBiX_6 (X = Cl, Br, I).

From TDOS figures, the VB and CB are mainly contributed by the Bi atoms and the corresponding halogen atoms (Cl, Br, I). The PDOS plots represent that, in the information of VB, the energy states corresponding to 6p electrons of Bi contribute scantily, while energy states corresponding to 4d electrons of Cs, 3p electrons of K and 3p/4p/5p electrons of Cl/Br/I take part significantly. In the conduction band, there is a major contribution of 6p states of Bi and 4d states of Cs for all three compounds. It has been observed that replacement of X-site anion gradually by Cl,

Br, and I cused a significant shift of the 6p states of Bi and 4d states of Cs towards the fermi level which caused a decrease in the bandgap value from 4.00 to 2.57 eV. This reducton in the bandgap value is attributed to more electronic states available in I due to its larger atomic mass as compared to Cl and Br.

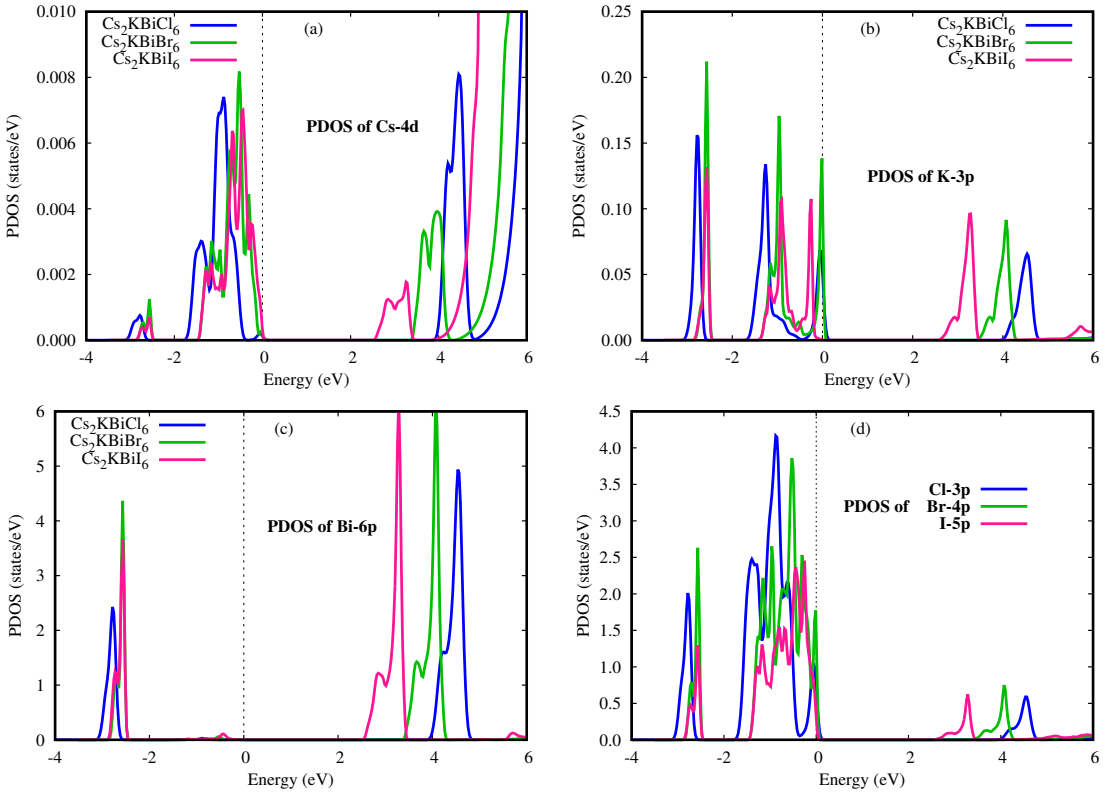

Figure 3.5: Partial density of states of double perovskites Cs_2KBiX_6 (X = Cl, Br, I).

Table 3.1: The calculated optimized structural parameters and bandgaps of Cs_2KBiX_6 (X = Cl, Br, I).

Compounds	Lattice Constant (Å)	Tolerance factor	Formation energy	Bandgap (eV)
Cs_2KBiCl_6	11.51	0.83	−2.08	4.00
Cs_2KBiBr_6	12.08	0.82	−1.69	3.42
Cs_2KBiI_6	12.94	0.81	−1.27	2.57

3.3 Optical properties

The interaction of light with matter can be used to study the optical performance of materials. The electromagnetic resonance between the incident light and the bound electrons in the valence band has an impact on the optical response. When energy is encountered, the bound electrons absorb it and move into the conduction band and the process of recombination is used to evaluate a material's potential for application in photovoltaic and other optoelectronic devices [87, 88]. We have analyzed the optical parameters of Cs_2KBiX_6 (X = Cl, Br, I) by computing complex dielectric function $\epsilon(\omega)$, absorption coefficient $\alpha(\omega)$, optical conductivity $\sigma(\omega)$, reflectivity $R(\omega)$, energy loss function $E_{loss}(\omega)$, refractive index $n(\omega)$, and extinction coefficient $k(\omega)$.

3.3.1 Complex Dielectric Function

The optical nature of any material is explained by the complex dielectric function which describes the relationship between a material's response to incident photons and its energy and is given by Ehrenreich and Cohen's equation state as follows [89]:

$$\epsilon(\omega) = \epsilon_1(\omega) + i\epsilon_2(\omega) \tag{3.4}$$

Here, the symbol ω represents the angular frequency of electromagnetic radiation that is incident on the specimen. Where, $\epsilon_1(\omega)$ is the real part and $\epsilon_2(\omega)$ is the imaginary part of the dielectric function. The real part explains the degree of polarization of a compound as a response to electromagnetic wave interactions whereas the imaginary part indicates loss factor or the absorption of incident light energy. The dielectric function's real component $\epsilon_1(\omega)$ and imaginary component $\epsilon_2(\omega)$ can be determined by using the Kramers-Kroning equation:

$$\epsilon_1(\omega) = 1 + \frac{2}{\pi} P \int_0^\infty \frac{\omega' \epsilon_2(\omega')}{\omega'^2 - \omega^2} d\omega \tag{3.5}$$

$$\epsilon_2(\omega) = \frac{e^2 h'}{\pi m^2 \omega^2} \Sigma_{\nu,c} \int_{BZ}^\infty |M_{c\nu}(k)|^2 \delta[\omega_{c\nu}(k) - \omega] d^3k \tag{3.6}$$

where, $M_{C\nu}(k) = \langle u_{ck}|e\nabla|u_{vk}\rangle$ is dipole matrix element expressing all the contributing electronic transitions. where P and k shows the principle quantum number and wave vector respectively, h is a Plank constant, ω is the angular frequency, and M is the molar mass of the carriers. The variation in real dielectric function ($\epsilon_1(\omega)$) of Cs_2KBiX_6 (X = Cl, Br, I) as a function of incident radiation's energy is represented in Figure 3.6(a). The real dielectric constants of the compounds are given by their static value i.e., $\epsilon_1(0)$ and found to be 2.90, 3.30, 4.10 for Cs_2KBiCl_6, Cs_2KBiBr_6, and Cs_2KBiI_6 respectively, which confirms that, substituting Cl with Br and I sequentially increases its response to electromagnetic radiation. From Figure 3.6 (a) it is also observed that, the value of $\epsilon_1(\omega)$ first gradually increasing with energy, then after reaching its maximum value at 3.8 eV (Cl), 3.2 eV (Br), and 2.8 eV (I) respectively. It drops down and again reaches a peak value at 4 eV (Cl), 4.1 eV (Br), and 3.7 eV (I) and after that turns out to be negative after 5 eV, 4.5 eV, and 4 eV for Cs_2KBiCl_6, Cs_2KBiBr_6, and Cs_2KBiI_6 respectively. The peak values of $\epsilon_1(\omega)$ indicate that, Cs_2KBiCl_6, Cs_2KBiBr_6 are of great interest in the ultraviolet (UV) range and Cs_2KBiI_6 is of great interest in the visible range of electromagnetic radiation. The negative dielectric constants represent the conductive characteristics of the studied compounds.

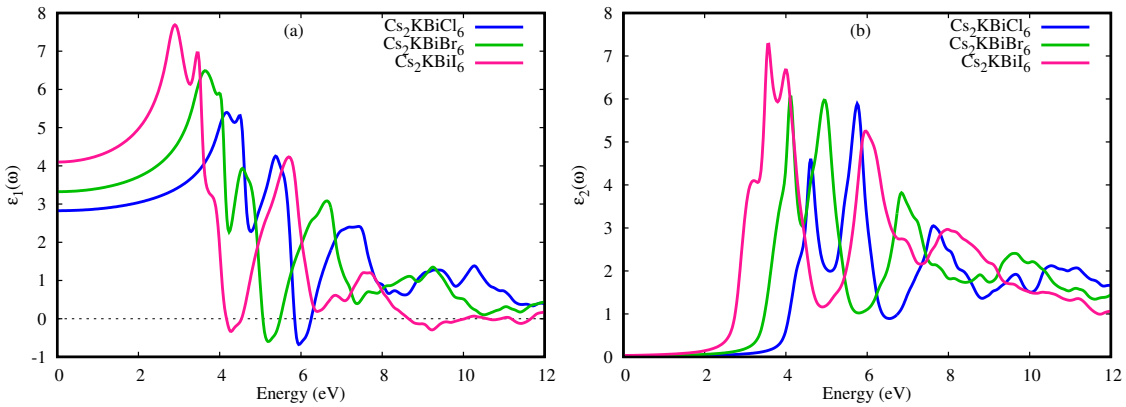

Figure 3.6: Complex dielectric function spectra of Cs_2KBiX_6 (X = Cl, Br, I) halide double perovskites. (a) Displays its real part-$\epsilon_1(\omega)$ and (b) displays its imaginary part-$\epsilon_2(\omega)$.

Figure 3.6 (b) represents the variation in imaginary dielectric function ($\epsilon_2(\omega)$) with the energy of incident radiation. It represents the radiation absorbed by the com-

pounds and their peaks explain the transition between the valence band maxima and conduction band minima. The threshold energy values of $\epsilon_2(\omega)$ for Cs_2KBiCl_6, Cs_2KBiBr_6, and Cs_2KBiI_6 are 3.9 eV, 3.2 eV, and 2.35 eV respectively, which indicate the optical bandgaps of the studied compounds and which are found to be very close to the electronic bandgaps of the compounds. The reasonable peaks of $\epsilon_2(\omega)$ reside on 3 eV to 8 eV for three compounds. Their increase occurs because at energies significantly higher than the bandgaps, the materials absorp a substantial amount of energy making the imaginary part of the dielectric function highly significant.

3.3.2 Absorption Coefficient and Optical Conductivity

The absorption coefficient $\alpha(\omega)$, is crucial for understanding how effectively a material absorbs light. Figure 3.7 (a) shows the variation of $\alpha(\omega)$ with the energy of incident radiation of the Cs_2KBiX_6 (X = Cl, Br, I) double perovskites. Electrons cannot transit from the valence band to the conduction band unless the energy of the incident light is lower than the bandgap energy of the material. The absorption starts at threshold energy of 3.8 eV (Cl), 3.1 eV (Br), and 2.3 eV (I) respectively which are very close to the electronic bandgaps of the materials. No absorption can be seen below the threshold energy which shows the materials transparency in this energy range. The absorption coefficient within the visible range is notably low,

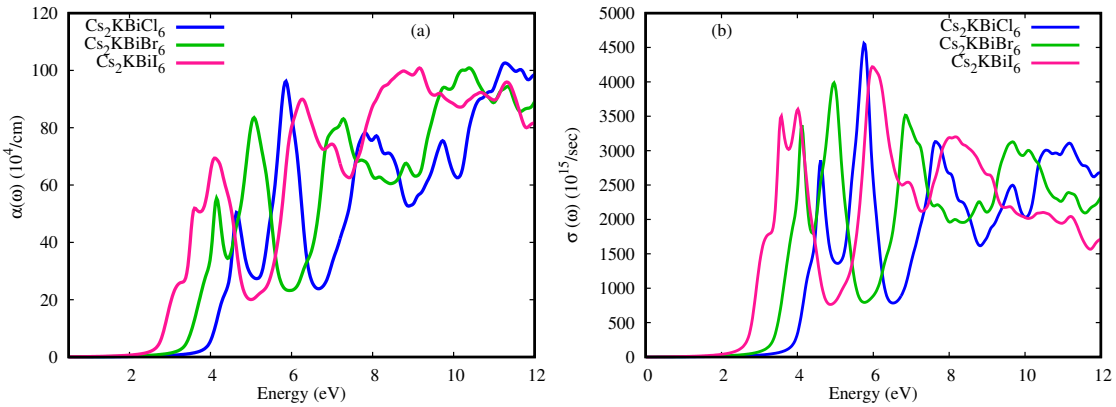

Figure 3.7: (a) Displays absorption coefficient-$\alpha(\omega)$ and (b) displays optical conductivity-$\sigma(\omega)$ of Cs_2KBiX_6 (X = Cl, Br, I) halide double perovskites.

suggesting an inability to absorb visible light. However, beyond the visible light energy range, there is an upsurge in absorption, indicating a preference for absorbing ultraviolet light. The highest peaks of $\alpha(\omega)$ are noticed between 4 and 12 eV for the considered double perovskites. So, for higher energies, more light will be absorbed by the materials.

The optical conductivity $\sigma(\omega)$ is the result of conduction of electrons when a photon of certain frequency falls on a material. The optical conductivity $\sigma(\omega)$, measured in ohm per centimeter of Cs_2KBiX_6 (X = Cl, Br, I) double perovskites is displayed in Figure 3.7 (b). The optical conductivity begins at 3.7 eV, 2.9 eV, and 2.0 eV for Cs_2KBiCl_6, Cs_2KBiBr_6, and Cs_2KBiI_6 respectively. The figure reveals that the optical conductivity increases initially and reaches a certain maximum value for each compound and then decreases again along the high energy range. The maximum value of the optical conductivity of Cs_2KBiCl_6 is 4600 $\times 10^{15}$/sec at 5.9 eV, Cs_2KBiBr_6 is 4000 $\times 10^{15}$/sec at 4.9 eV and Cs_2KBiI_6 is 4300 $\times 10^{15}$/sec at 6 eV respectively. The broad range of $\sigma(\omega)$ for all the compounds lie in a wide energy range at 4 eV to 12 eV, showing their potential to use in optoelectronic in ultraviolet range. It is observed that optical conductivity and absorption show their minima and maxima in a similar region, which confirms the theoretical concept and thus the accuracy of the computed results.

3.3.3 Reflectivity and Electron Energy Loss

A fraction of energy which bounces back from the material medium is calculated as reflectivity $R(\omega)$. The energy dependent $R(\omega)$ dispersion for the studied double perovskites is shown in Figure 3.8 (a). It represents that, the static values of reflectivity $R(0)$ are 7%, 8%, and 12% for Cs_2KBiCl_6, Cs_2KBiBr_6, and Cs_2KBiI_6 respectively. The static value of reflectivity increases when we substitute small sized anion Cl with large sized anion I. The maximum value of reflectivity of Cs_2KBiCl_6 is 32% at 5.8 eV, Cs_2KBiBr_6 is 32% at 4.9 eV and Cs_2KBiI_6 is 32% at 4.1 eV. the maximum values of reflectivity are same for three compounds at different energy range and the peaks are shown in ultraviolet (UV) region. This reflectivity values are associated with real dielectric constant because highest reflectivity is exhibited for the energy

values where negative $\epsilon(\omega)$ is exhibited.

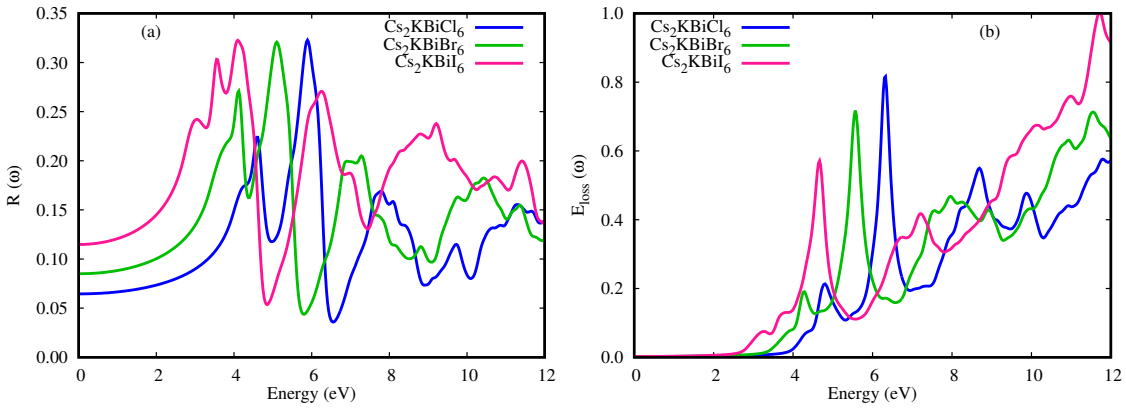

Figure 3.8: (a) Displays reflectivity-R(ω) and (b) displays energy loss function-$E_{loss}(\omega)$ of Cs_2KBiX_6 (X = Cl, Br, I) halide double perovskites.

Electron energy loss (EEL) refers to the amount of energy that an electron loses while traversing a substance. The plot for electron energy loss for Cs_2KBiX_6 (X = Cl, Br, I) double perovskites has been shown in Figure 3.8 (b). The peaks in energy loss spectrum occur at those values of incident energy of photons where reflectivity suddenly decreases. The figure illustrates that the loss increases with increasing energy.

3.3.4 Refractive Index

The refractive index $n(\omega)$ is also a significant optical parameter that relates to the transparency of materials. In other words, $n(\omega)$ is a fundamental property of a material that indicates how light is bent or refracted within a material. The variation of refractive index with the energy of incident radiation is depicted in Figure 3.9 (a). The static value of refractive index $n(0)$ of Cs_2KBiX_6 are 1.65 (Cl), 1.8 (Br), and 2.1 (I) respectively. Initially, $n(\omega)$ gradually increases and reaches peak value at 4.2 eV (Cl), 4.0 eV (Br), and 3.7 eV (I). The peak values shift towards lower energy range with the replacement of Cl with Br and I. So, these three materials show peak value in the ultraviolet region. Beyond the peak values, variations occur which depicts that light enter into the materials. These peaks explain the transition of electron between the valence band maxima and conduction band minima. Moreover, the

variations indicate the lower transparency of the compounds in high region.

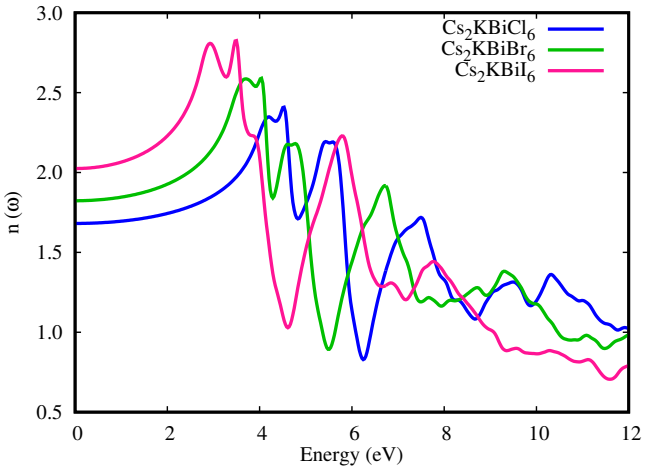

Figure 3.9: Displays refractive index-n(ω) of Cs_2KBiX_6 (X = Cl, Br, I) halide double perovskites.

3.4 Thermoelectric properties

The efficiency of converting thermal energy to electric energy in Cs_2KBiX_6 (X = Cl, Br, I) double perovskites can be evaluated by analyzing their thermoelectric properties with the BoltzTraP code. Reducing environmental pollution and preventing energy crises, thermoelectric materials are of great interest transforming wasted heat into useful electricity [90–92]. Thermoelectric parameters, such as electrical (σ/τ) and thermal (κ/τ) conductivities as well as the Seebeck coefficient (S), power factor (PF) and figure of merit (ZT). The relaxation time (τ) is considered as a constant which is a good approximation for the carrier processes independent of the reciprocal lattice vector and temperature.

3.4.1 Electrical Conductivity

The electrical conductivity per unit relaxation time (σ/τ) against temperature T (100-1000 K) of the Cs_2KBiX_6 (X = Cl, Br, I) double perovskites is displayed in Figure 3.10. The calculated results indicate a linear increase in σ/τ with increasing temperature. We can also say that, electrical resistivity decreases with rise in tem-

perature signifying negative temperature coefficient of resistivity, which confirms the semiconductor nature of the compounds [93]. Increasing the temperature leads to a higher intrinsic carrier concentration. The values of electrical conductivity at 1000 K increases from $0.42 \times 10^{19}(\Omega.m.s)^{-1}$ to $0.7 \times 10^{19}(\Omega.m.s)^{-1}$ to $1.19 \times 10^{19}(\Omega.m.s)^{-1}$ while moving from Cl to Br to I, seemingly because of the larger sizes of anion.

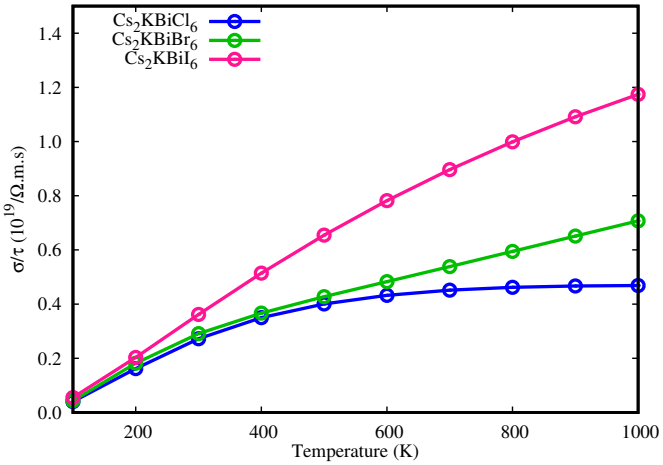

Figure 3.10: Variation in electrical conductivity per unit relaxation time with temperature of halide double perovskites Cs_2KBiX_6 (X = Cl, Br, I).

3.4.2 Thermal Conductivity

Figure 3.11 represents thermal conductivity per unit relaxation time (κ/τ) varying against temperature for all the three studied double perovskites. It is evident from the graph that κ/τ increases with temperature. There is negligible difference in κ/τ for all the compounds upto 200 K. Beyond this temperature, the difference becomes prominent and conductivity increases linearly. The rate of increase of κ/τ is faster than σ/τ with temperature. The increase in the value of κ/τ with temperature indicates that at a higher temperature more lattice vibrations are generated, which causes an increase in κ/τ [94]. At higher temperature, Cs_2KBiCl_6 has the lowest conductivity among the three compounds, indicating its potential to use in thermoelectric applications as compared to the other two.

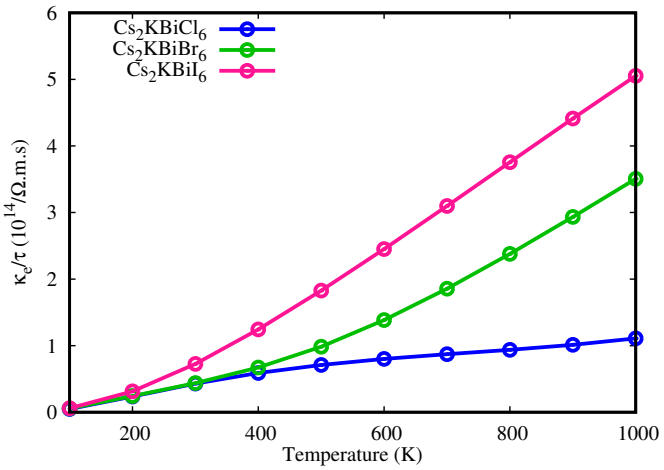

Figure 3.11: Variation in thermal conductivity per unit relaxation time with temperature of halide double perovskites Cs_2KBiX_6 (X = Cl, Br, I).

3.4.3 Seebeck Coefficient

The ratio of the voltage produced to the temperature gradient is known as Seebeck coefficient (S). Seebeck coefficient determines the ability of a material to generate the electromotive force from the applied temperature gradient through the material, in other words it indicates the effectiveness of the thermocouples [95]. Seebeck coefficient (S) against temperature (T) is presented in Figure 3.12.

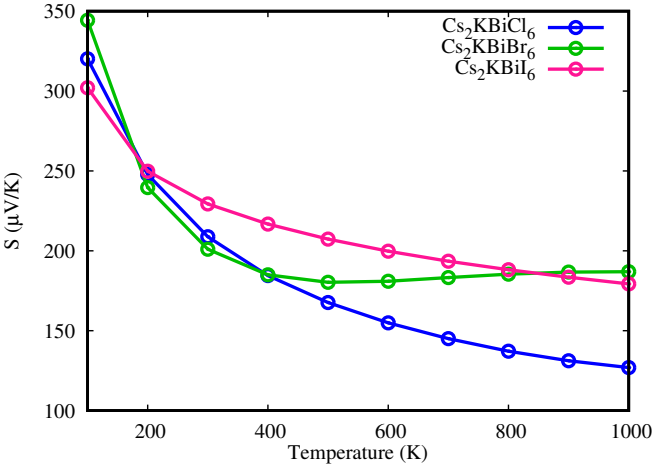

Figure 3.12: Variation in Seebeck coefficient with temperature of halide double perovskites Cs_2KBiX_6 (X = Cl, Br, I).

The positive values of S for Cs_2KBiX_6 (X = Cl, Br, I) double perovskites reveal

that positive charge carriers are the majority charge carriers in three materials. In the Figure 3.12, the value of Seebeck coefficient decreases from 320 μV/k to 125 μV/k for Cs_2KBiCl_6, from 348 μV/k to 190 μV/k for Cs_2KBiBr_6 and from 300 μV/k to 180 μV/k for Cs_2KBiI_6 respectively. Because in this temperature range, increasing σ/τ decreases the potential barrier. The value of S $\geq$ 200 μV/k are indicative of the excellent thermoelectric materials [96]. In our calculation, at room temperature, the values of Seebeck coefficient are 210 μV/k, 200 μV/k, and 230 μV/k for Cs_2KBiCl_6, Cs_2KBiBr_6, Cs_2KBiI_6 respectively, which are remarkably outstanding to the mentioned value. The positive values of Seebeck coefficient reveal the p-type semiconductor nature of these double perovskites. Therefore, the studied double perovskite materials have excellent potential for thermoelectric applications.

3.4.4 Power Factor

Power factor (PF) plays a vital role in determining the thermoelectric efficiency of a material. It is a collective effect of S and σ, which is calculated by the expression PF = $S^2\sigma$. The temperature-dependent variation of PF is shown in Figure 3.13.

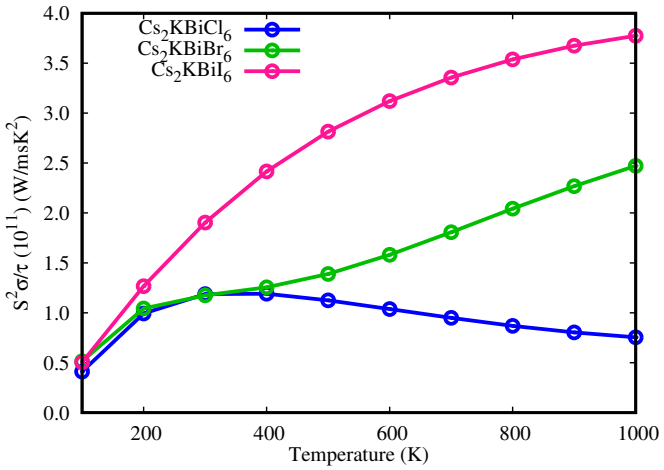

Figure 3.13: Variation in power factor with temperature of halide double perovskites Cs_2KBiX_6 (X = Cl, Br, I).

Their room temperature (300 K) values increases from 1.2×10^{11} W/msK^2 to 2×10^{11} W/msK^2 while moving from Cl to I. The maximum values of PF are 1.2×10^{11} W/msK^2, 2.5×10^{11} W/msK^2, and 3.8×10^{11} W/msK^2 for Cs_2KBiCl_6, Cs_2KBiBr_6,

and Cs_2KBiI_6 respectively. The values of PF of Cs_2KBiBr_6 and Cs_2KBiI_6 increase with increasing the temperature, and the value of PF of Cs_2KBiCl_6 increase upto 300 K and beyond this temperature the PF value decreases with increasing temperature.

3.4.5 Figure Of Merit

Most important among the thermoelectric parameters in the figure of merit (ZT). It determines the efficiency of thermoelectric devices and is calculated using the expression $ZT = S^2\sigma T/\kappa$, where S, σ, κ and T represent the Seebeck coefficient, electronic conductivity, thermal conductivity and temperature in kelvin, respectively [97].

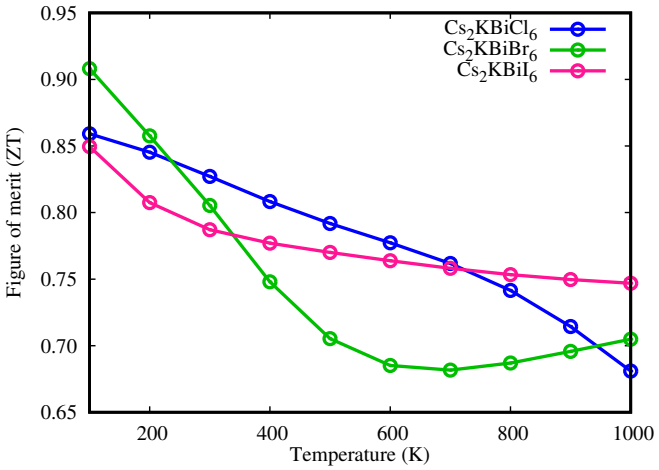

Figure 3.14: Variation in power factor with temperature of halide double perovskites Cs_2KBiX_6 (X = Cl, Br, I).

The variation of ZT for Cs_2KBiX_6 (X = Cl, Br, I) double perovskites in the temperature range 100-1000 K is represented in Figure 3.14. The ZT value at 100 K are 0.86, 0.91, 0.85 for Cs_2KBiCl_6, Cs_2KBiBr_6, and Cs_2KBiI_6 respectively. ZT decreases with increasing temperature (300 K), the value of ZT are 0.83 (Cl), 0.81 (Br), and 0.79 (I) respectively. With further increment of temperature, ZT decreases gradually. These observations indicate that, these double perovskites are good candidates to use in thermoelectric applications based on their ZT values obtained in our calculations.

Chapter 4

Conclusions

In this work, we have investigated the structural, electronic, optical and thermoelectric properties of double perovskites Cs_2KBiX_6 (X = Cl, Br, I) through first-principles study. The structural stabilities of these materials are estimated based on the values of the tolerance factors and octahedral factors. The energy volume optimization graphs are showed that the replacement of X-site anion sequentially by Cl, Br, and I caused an expansion in the lattice constant due to the larger ionic radius of Br and I. The lattice constant of three compounds are estimated to be 11.51 Å, 12.08 Å and 12.94 Å respectively. Among three compounds, Cs_2KBiCl_6 and Cs_2KBiBr_6 have direct bandgaps and Cs_2KBiI_6 possesses indirect bandgap. The bandgap of Cs_2KBiCl_6 is 4.00 eV, which reduced to 3.42 eV and 2.57 eV for Cs_2KBiBr_6 and Cs_2KBiI_6. Analysis of the density of states (DOS) reveal that, for all three compounds valence band and conduction band are mainly contributed by the Bi atoms and the corresponding halogen atoms (Cl, Br, I). The broad optical absorption and optical conductivity regions for all the three compounds lie in an energy range of 4 to 12 eV. The thermal and electrical conductivities were found to increase with temperature. The positive values of Seebeck coefficient reveal the p-type semiconductor nature of these double perovskites. At room temperature, the values of Seebeck coefficient are 210 μV/k, 200 μV/k and 230 μV/k respectively for

these studied compounds. The maximum values of the figure of merit are 0.86, 0.91, 0.85 for Cs_2KBiCl_6, Cs_2KBiBr_6, and Cs_2KBiI_6, respectively. The high optical absorption and optical conductivities, high electrical conductivities, positive Seebeck coefficient, and the optimum figure of merit make these compounds suitable for optoelectronic and thermoelectric applications including ultraviolet sensors, detectors, light emitting diodes, thermoelectric generators and coolers.

Bibliography

[1] Hong Wang, Muhammad Asif Amjad, Noman Arshed, Abdullah Mohamed, Shamsher Ali, Muhammad Afaq Haider Jafri, and Yousaf Ali Khan. Retracted: Fossil energy demand and economic development in BRICS countries. *Frontiers in Energy Research*, 10:842793, 2022.

[2] Christian Bogmans, Lama Kiyasseh, Akito Matsumoto, and Andreas Pescatori. Energy, efficiency gains and economic development: when will global energy demand saturate? 2020.

[3] Muhammad Kamran Khan, Muhammad Imran Khan, and Muhammad Rehan. The relationship between energy consumption, economic growth and carbon dioxide emissions in Pakistan. *Financial Innovation*, 6(1):1, 2020.

[4] Loiy Al-Ghussain. Global warming: review on driving forces and mitigation. *Environmental Progress & Sustainable Energy*, 38(1):13–21, 2019.

[5] Phebe Asantewaa Owusu and Samuel Asumadu-Sarkodie. A review of renewable energy sources, sustainability issues and climate change mitigation. *Cogent Engineering*, 3(1):1167990, 2016.

[6] Wei Zhang, Giles E Eperon, and Henry J Snaith. Metal halide perovskites for energy applications. *Nature Energy*, 1(6):1–8, 2016.

[7] Wan-Jian Yin, Tingting Shi, and Yanfa Yan. Unique properties of halide perovskites as possible origins of the superior solar cell performance. *Advanced Materials (Deerfield Beach, Fla.)*, 26(27):4653–4658, 2014.

[8] Jinwoo Byun, Himchan Cho, Christoph Wolf, Mi Jang, Aditya Sadhanala, Richard H Friend, Hoichang Yang, and Tae-Woo Lee. Efficient visible quasi-2d

perovskite light-emitting diodes. *Advanced Materials (Deerfield Beach, Fla.)*, 28(34):7515–7520, 2016.

[9] Jianhai Li, Leimeng Xu, Tao Wang, Jizhong Song, Jiawei Chen, Jie Xue, Yuhui Dong, Bo Cai, Qingsong Shan, Boning Han, et al. 50-fold eqe improvement up to 6.27% of solution-processed all-inorganic perovskite $CsPbBr_3$ qleds via surface ligand density control. *Advanced Materials*, 29(5):1603885, 2017.

[10] Haiming Zhu, Yongping Fu, Fei Meng, Xiaoxi Wu, Zizhou Gong, Qi Ding, Martin V Gustafsson, M Tuan Trinh, Song Jin, and XY Zhu. Lead halide perovskite nanowire lasers with low lasing thresholds and high quality factors. *Nature Materials*, 14(6):636–642, 2015.

[11] Parthiban Ramasamy, Da-Hye Lim, Bumjin Kim, Seung-Ho Lee, Min-Sang Lee, and Jong-Soo Lee. All-inorganic cesium lead halide perovskite nanocrystals for photodetector applications. *Chemical Communications*, 52(10):2067–2070, 2016.

[12] Kin Mun Wong. Characterization, modeling and physical mechanisms of different surface treatment methods at room temperature on the oxide and interfacial quality of the SiO_2 film using the spectroscopic scanning capacitance microscopy. *Results in Physics*, 7:1308–1318, 2017.

[13] Sami Vasala and Maarit Karppinen. A_2BBO_6 perovskites: a review. *Progress in Solid State Chemistry*, 43(1-2):1–36, 2015.

[14] Guichuan Xing, Nripan Mathews, Shuangyong Sun, Swee Sien Lim, Yeng Ming Lam, Michael Grätzel, Subodh Mhaisalkar, and Tze Chien Sum. Long-range balanced electron-and hole-transport lengths in organic-inorganic $CH_3NH_3PbI_3$. *Science*, 342(6156):344–347, 2013.

[15] Giacomo Giorgi, Jun-Ichi Fujisawa, Hiroshi Segawa, and Koichi Yamashita. Small photocarrier effective masses featuring ambipolar transport in methylammonium lead iodide perovskite: a density functional analysis. *The Journal of Physical Chemistry Letters*, 4(24):4213–4216, 2013.

[16] Kyle Frohna, Tejas Deshpande, John Harter, Wei Peng, Bradford A Barker, Jeffrey B Neaton, Steven G Louie, Osman M Bakr, David Hsieh, and Marco Bernardi. Inversion symmetry and bulk rashba effect in methylammonium lead iodide perovskite single crystals. *Nature Communications*, 9(1):1829, 2018.

[17] Sadia Ameen, Malik Abdul Rub, Samia A Kosa, Khalid A Alamry, M Shaheer Akhtar, Hyung-Shik Shin, Hyung-Kee Seo, Abdullah M Asiri, and Mohammad Khaja Nazeeruddin. Perovskite solar cells: influence of hole transporting materials on power conversion efficiency. *ChemSusChem*, 9(1):10–27, 2016.

[18] Joseph S Manser, Makhsud I Saidaminov, Jeffrey A Christians, Osman M Bakr, and Prashant V Kamat. Making and breaking of lead halide perovskites. *Accounts of Chemical Research*, 49(2):330–338, 2016.

[19] Weijun Ke and Mercouri G Kanatzidis. Prospects for low-toxicity lead-free perovskite solar cells. *Nature Communications*, 10(1):965, 2019.

[20] Qianqian Fan, Gill V Biesold-McGee, Jianzhong Ma, Qunna Xu, Shuang Pan, Juan Peng, and Zhiqun Lin. Lead-free halide perovskite nanocrystals: crystal structures, synthesis, stabilities, and optical properties. *Angewandte Chemie International Edition*, 59(3):1030–1046, 2020.

[21] Zewen Xiao, Zhaoning Song, and Yanfa Yan. From lead halide perovskites to lead-free metal halide perovskites and perovskite derivatives. *Advanced Materials*, 31(47):1803792, 2019.

[22] Wen-Fan Yang, Femi Igbari, Yan-Hui Lou, Zhao-Kui Wang, and Liang-Sheng Liao. Tin halide perovskites: progress and challenges. *Advanced Energy Materials*, 10(13):1902584, 2020.

[23] Weijun Ke, Constantinos C Stoumpos, and Mercouri G Kanatzidis. "unleaded" perovskites: status quo and future prospects of tin-based perovskite solar cells. *Advanced Materials*, 31(47):1803230, 2019.

[24] Elizabeth S Parrott, Rebecca L Milot, Thomas Stergiopoulos, Henry J Snaith, Michael B Johnston, and Laura M Herz. Effect of structural phase transition on charge-carrier lifetimes and defects in $CH_3NH_3SnI_3$ perovskite. *The Journal of Physical Chemistry Letters*, 7(7):1321–1326, 2016.

[25] Nacereddine Lakhdar and Abdelkader Hima. Electron transport material effect on performance of perovskite solar cells based on $CH_3NH_3GeI_3$. *Optical Materials*, 99:109517, 2020.

[26] Lester R Morss, M Siegal, L Stenger, and Norman Edelstein. Preparation of cubic chloro complex compounds of trivalent metals: Cs_2NaMCl_6. *Inorganic Chemistry*, 9(7):1771–1775, 1970.

[27] Adam H Slavney, Te Hu, Aaron M Lindenberg, and Hemamala I Karunadasa. A bismuth-halide double perovskite with long carrier recombination lifetime for photovoltaic applications. *Journal of the American Chemical Society*, 138(7):2138–2141, 2016.

[28] Baoning Wang, Na Li, Lin Yang, Chunxiang Dall'Agnese, Ajay Kumar Jena, Tsutomu Miyasaka, and Xiao-Feng Wang. Organic dye/$Cs_2AgBiBr_6$ double perovskite heterojunction solar cells. *Journal of the American Chemical Society*, 143(36):14877–14883, 2021.

[29] Lei Zhou, Yang-Fan Xu, Bai-Xue Chen, Dai-Bin Kuang, and Cheng-Yong Su. Synthesis and photocatalytic application of stable lead-free $Cs_2AgBiBr_6$ perovskite nanocrystals. *Small*, 14(11):1703762, 2018.

[30] Haoran Li, Xin Shan, Jennifer N Neu, Thomas Geske, Melissa Davis, Pengsu Mao, Kai Xiao, Theo Siegrist, and Zhibin Yu. Lead-free halide double perovskite-polymer composites for flexible X-ray imaging. *Journal of Materials Chemistry C*, 6(44):11961–11967, 2018.

[31] Julian A Steele, Weicheng Pan, Cristina Martin, Masoumeh Keshavarz, Elke Debroye, Haifeng Yuan, Subhasree Banerjee, Eduard Fron, Dries Jonckheere, Cheol Woong Kim, et al. Photophysical pathways in highly sensitive $Cs_2AgBiBr_6$ double-perovskite single-crystal x-ray detectors. *Advanced Materials*, 30(46):1804450, 2018.

[32] Eric T McClure, Molly R Ball, Wolfgang Windl, and Patrick M Woodward. Cs_2AgBiX_6 (X= Br, Cl): new visible light absorbing, lead-free halide perovskite semiconductors. *Chemistry of Materials*, 28(5):1348–1354, 2016.

[33] Muhammad Waqas Iqbal, Mumtaz Manzoor, NA Noor, Ibadur Rehman, Nohseen Mushahid, Sikandar Aftab, Yousef Muhammad Alanazi, Hamid Ullah, and Amir Muhammad Afzal. Tuning of the electronic bandgap of lead-free double perovskites K_2AgBiX_6 (X= Cl, Br) for solar cells applications and their thermoelectric characteristics. *Solar Energy*, 239:234–241, 2022.

[34] Q Mahmood, Taharh Zelai, M Hassan, Ghazanfar Nazir, Hind Albalawi, N Sfina, Nessrin A Kattan, A Hakamy, Abeer Mera, and Mohammed A Amin. Study of lead-free double perovskites X_2AgBiI_6 (X= K, Rb, Cs) for solar cells and thermoelectric applications. *Journal of Materials Research and Technology*, 22:913–922, 2023.

[35] Marina R Filip, Xinlei Liu, Anna Miglio, Geoffroy Hautier, and Feliciano Giustino. Phase diagrams and stability of lead-free halide double perovskites Cs_2BBX_6: B= Sb and Bi, B= Cu, Ag, and Au, and X= Cl, Br, and I. *The Journal of Physical Chemistry C*, 122(1):158–170, 2018.

[36] Syed Zuhair Abbas Shah, Shanawer Niaz, Tabassum Nasir, and James Sifuna. First principles insight into band gap tuning in bismuth based double perovskites $X_2NaBiCl_6$ (X= Cs, Rb, K) for enhanced optoelectronic and thermoelectric properties. *Results in Chemistry*, 5:100828, 2023.

[37] Peter Blaha, Karlheinz Schwarz, P Sorantin, and SB Trickey. Full-potential, linearized augmented plane wave programs for crystalline systems. *Computer Physics Communications*, 59(2):399–415, 1990.

[38] Peter Blaha, Karlheinz Schwarz, Fabien Tran, Robert Laskowski, Georg KH Madsen, and Laurence D Marks. Wien2k: An APW+lo program for calculating the properties of solids. *The Journal of Chemical Physics*, 152(7), 2020.

[39] David J Griffiths and Darrell F Schroeter. *Introduction to quantum mechanics*. Cambridge university press, 2018.

[40] Max Born. Quantenmechanik der stoßvorgänge. *Zeitschrift für physik*, 38(11-12):803–827, 1926.

[41] Stefan Blügel and Gustav Bihlmayer. Full-potential linearized augmented planewave method. *Computational Nanoscience: do it yourself*, 31:85–129, 2006.

[42] David J Griffiths and Darrell F Schroeter. *Introduction to quantum mechanics*. Cambridge university press, 2018.

[43] GEORGE NIKOULIS and JOSEPH KIOSEOGLOU. Computational analysis of charge distribution of Pd nanoparticles on Mg and MgO substrates.

[44] E Schrödinger. Schrödinger 1926e. *Annalen Der Physik*, 81:109, 1926.

[45] DJ Griffiths. Introduction to quantum mechanics 2nd ed.-solutions. 2005.

[46] Max Born. Quantenmechanik der stoßvorgänge. *Zeitschrift für Physik*, 38(11):803–827, 1926.

[47] David C Young. Density functional theory. *Computational Chemistry*, pages 42–48, 2001.

[48] Wolfgang Pauli. The connection between spin and statistics. *Physical Review*, 58(8):716, 1940.

[49] Arthur Jabs. Connecting spin and statistics in quantum mechanics. *Foundations of Physics*, 40(7):776–792, 2010.

[50] Attila Szabo and Neil S Ostlund. *Modern quantum chemistry: introduction to advanced electronic structure theory*. Courier Corporation, 2012.

[51] Wolfgang Pauli. On the connexion between the completion of electron groups in an atom with the complex structure of spectra. *Zeitschrift für Physik*, 31:765, 1925.

[52] Nouredine Zettili. Quantum mechanics: concepts and applications. 2003.

[53] E BRoDA. Nuclear chemistry. *Chemistry To-day: A Guide for Teachers: Selected Topics for a Modern Approach to the Teaching of School Chemistry*, page 335, 1963.

[54] Niklas Zwettler. Density functional theory.

[55] F Schwabl. Quantum mechanics (QM I). ; Quantenmechanik (QM I). Eine Einfuehrung. 2007.

[56] Franz Schwabl. *Quantenmechanik (QM I): Eine Einführung*. Springer-Verlag, 2013.

[57] Paul Adrien Maurice Dirac. A new notation for quantum mechanics. 35(3):416–418, 1939.

[58] Christian B Lang and Norbert Pucker. *Mathematische methoden in der physik*, volume 2. Springer, 2005.

[59] Wolfram Koch and Max C Holthausen. *A chemist's guide to density functional theory*. John Wiley & Sons, 2015.

[60] Walter Kohn. Nobel lecture: Electronic structure of matter—wave functions and density functionals. *Reviews of Modern Physics*, 71(5):1253, 1999.

[61] Per-Olov Löwdin. Scaling problem, virial theorem, and connected relations in quantum mechanics. *Journal of Molecular Spectroscopy*, 3(1-6):46–66, 1959.

[62] Pierre Hohenberg and Walter Kohn. Inhomogeneous electron gas. *Physical Review*, 136(3B):B864, 1964.

[63] Michael P Marder. *Condensed matter physics*. John Wiley & Sons, 2010.

[64] Mathieu Lewin, Elliott H Lieb, and Robert Seiringer. The local density approximation in density functional theory. *Pure and Applied Analysis*, 2(1):35–73, 2019.

[65] Reiner M Dreizler and Eberhard KU Gross. *Density functional theory: an approach to the quantum many-body problem*. Springer Science & Business Media, 2012.

[66] Klaus Capelle, Carsten A Ullrich, and Giovanni Vignale. Degenerate ground states and nonunique potentials: Breakdown and restoration of density functionals. *Physical Review A*, 76(1):012508, 2007.

[67] John A Pople, Peter MW Gill, and Benny G Johnson. Kohn—sham density-functional theory within a finite basis set. *Chemical Physics Letters*, 199(6):557–560, 1992.

[68] John P Perdew. Generalized gradient approximations for exchange and correlation: A look backward and forward. *Physica B: Condensed Matter*, 172(1-2):1–6, 1991.

[69] Axel D Becke. Density-functional exchange-energy approximation with correct asymptotic behavior. *Physical Review A*, 38(6):3098, 1988.

[70] John P Perdew, John A Chevary, Sy H Vosko, Koblar A Jackson, Mark R Pederson, Dig J Singh, and Carlos Fiolhais. Atoms, molecules, solids, and surfaces: Applications of the generalized gradient approximation for exchange and correlation. *Physical Review B*, 46(11):6671, 1992.

[71] Ulf Von Barth and Lars Hedin. A local exchange-correlation potential for the spin polarized case. i. *Journal of Physics C: Solid State Physics*, 5(13):1629, 1972.

[72] John P Perdew, Jianmin Tao, Viktor N Staroverov, and Gustavo E Scuseria. Meta-generalized gradient approximation: Explanation of a realistic nonempirical density functional. *The Journal of Chemical Physics*, 120(15):6898–6911, 2004.

[73] Yan Zhao and Donald G Truhlar. The $M0_6$ suite of density functionals for main group thermochemistry, thermochemical kinetics, noncovalent interactions, excited states, and transition elements: two new functionals and systematic testing of four $M0_6$-class functionals and 12 other functionals. *Theoretical Chemistry Accounts*, 120:215–241, 2008.

[74] Jianwei Sun, Adrienn Ruzsinszky, and John P Perdew. Strongly constrained and appropriately normed semilocal density functional. *Physical Review Letters*, 115(3):036402, 2015.

[75] Vladimir I Anisimov, Ferdi Aryasetiawan, and AI Lichtenstein. First-principles calculations of the electronic structure and spectra of strongly correlated systems: the LDA+ U method. *Journal of Physics: Condensed Matter*, 9(4):767, 1997.

[76] MT Czyżyk and GA Sawatzky. Local-density functional and on-site correlations: The electronic structure of La_2CuO_4 and $LaCuO_3$. *Physical Review B*, 49(20):14211, 1994.

[77] Vlasdimir I Anisimov, IV Solovyev, MA Korotin, MT Czyżyk, and GA Sawatzky. Density-functional theory and NiO photoemission spectra. *Physical Review B*, 48(23):16929, 1993.

[78] Erik R Ylvisaker, Warren E Pickett, and Klaus Koepernik. Anisotropy and magnetism in the LSDA+U method. *Physical Review B—Condensed Matter and Materials Physics*, 79(3):035103, 2009.

[79] Georg KH Madsen and David J Singh. BoltzTraP. a code for calculating bandstructure dependent quantities. *Computer Physics Communications*, 175(1):67–71, 2006.

[80] John P Perdew, Kieron Burke, and Matthias Ernzerhof. Generalized gradient approximation made simple. *Physical Review Letters*, 77(18):3865, 1996.

[81] Walter Kohn and L Sham. Density functional theory. 49:561–572, 1996.

[82] Upasana Rani, Peeyush Kumar Kamlesh, Rohit Agarwal, Jyoti Kumari, and Ajay Singh Verma. Electronic and thermo-physical properties of double antiperovskites X_6SOA_2 (X= Na, K and A= Cl, Br, I): A non-toxic and efficient energy storage materials. *International Journal of Quantum Chemistry*, 121(19):e26759, 2021.

[83] M Kibbou, Z Haman, I Bouziani, Nabil Khossossi, Y Benhouria, I Essaoudi, Abdelmajid Ainane, and Rajeev Ahuja. Cs_2InGaX_6 (X= Cl, Br, or I): emergent inorganic halide double perovskites with enhanced optoelectronic characteristics. *Current Applied Physics*, 21:50–57, 2021.

[84] Alexander E Fedorovskiy, Nikita A Drigo, and Mohammad Khaja Nazeeruddin. The role of goldschmidt's tolerance factor in the formation of A_2BX_6 double halide perovskites and its optimal range. *Small Methods*, 4(5):1900426, 2020.

[85] Chonghe Li, Kitty Chi Kwan Soh, and Ping Wu. Formability of ABO_3 perovskites. *Journal of Alloys and Compounds*, 372(1-2):40–48, 2004.

[86] Chonghea Li, Xionggang Lu, Weizhong Ding, Liming Feng, Yonghui Gao, and Ziming Guo. Formability of ABX_3 (X= F, Cl, Br, I) halide perovskites. *Acta Crystallographica Section B: Structural Science*, 64(6):702–707, 2008.

[87] Lalhriatpuia Hnamte, Sandeep Sandeep, Himanshu Joshi, and RK Thapa. Electronic and optical properties of double perovskite Ba_2VMoO_6: FP-LAPW study. 1953(1), 2018.

[88] Yao Cai, Wei Xie, Yin Ting Teng, Padinhare Cholakkal Harikesh, Biplab Ghosh, Patrick Huck, Kristin A Persson, Nripan Mathews, Subodh G Mhaisalkar, Matthew Sherburne, et al. High-throughput computational study of halide double perovskite inorganic compounds. *Chemistry of Materials*, 31(15):5392–5401, 2019.

[89] Sunita Kumari, Peeyush Kumar Kamlesh, Lalit Kumari, Sudhir Kumar, Sarita Kumari, Rashmi Singh, Rajeev Gupta, Manendra S Chauhan, Upasana Rani, and Ajay Singh Verma. Progress in theoretical study of lead-free halide double perovskite Na_2AgSbX_6 (X= F, Cl, Br, and I) thermoelectric materials. *Journal of Molecular Modeling*, 29(6):195, 2023.

[90] Yingzhi Zhou, Jing Wang, Dongxiang Luo, Dehua Hu, Yonggang Min, and Qifan Xue. Recent progress of halide perovskites for thermoelectric application. *Nano Energy*, 94:106949, 2022.

[91] Sile Hu, Zhilin Ren, Aleksandra B Djurisic, and Andrey L Rogach. Metal halide perovskites as emerging thermoelectric materials. *ACS Energy Letters*, 6(11):3882–3905, 2021.

[92] Andreas Kaltzoglou and Polycarpos Falaras. Recent developments on hybrid perovskite materials for solar energy conversion and environmental protection. *Current Opinion in Chemical Engineering*, 33:100708, 2021.

[93] NA Noor, Q Mahmood, M Rashid, Bakhtiar Ul Haq, and A Laref. The pressure-induced mechanical and optoelectronic behavior of cubic perovskite $PbSnO_3$ via ab-initio investigations. *Ceramics International*, 44(12):13750–13756, 2018.

[94] NA Noor, SM Alay-e Abbas, M Hassan, I Mahmood, ZA Alahmed, and AH Reshak. The under-pressure behaviour of mechanical, electronic and optical properties of calcium titanate and its ground state thermoelectric response. *Philosophical Magazine*, 97(22):1884–1901, 2017.

[95] A Shankar, DP Rai, Sandeep Chettri, R Khenata, and RK Thapa. FP-LAPW calculations of the elastic, electronic and thermoelectric properties of the filled skutterudite $CeRu_4Sb_{12}$. *Journal of Solid State Chemistry*, 240:126–132, 2016.

[96] Thi Kim Phuong Luong, Vinh Le Thanh, Abdelhamid Ghrib, Moustafa El Kurdi, and Philippe Boucaud. Making germanium, an indirect band gap semiconductor, suitable for light-emitting devices. *Advances in Natural Sciences: Nanoscience and Nanotechnology*, 6(1):015013, 2015.

[97] W Tahir, Ghulam M Mustafa, NA Noor, Syed Muhammad Alay-e Abbas, Q Mahmood, and A Laref. Analysis of optoelectronic and trasnport properties of magnesium based $MgSc_2X_4$ (X= S, Se) spinels for solar cell and energy storage device applications. *Ceramics International*, 46(17):26637–26645, 2020.